APPENDIX D
COLLISION ANYALYSIS

TO THE

INDEPENDENT RISK ANALYSIS
(APPENDIX C1)

Note: The U.S. Coast Guard has determined that this report contains sensitive security information (SSI) that cannot be made available to the general public. The complete report is available for review by Federal, State, and local agency staffs and elected officials with safety and security responsibilities and clearances. This report contains the following appendices:

A: Paper on Numerical Simulation of Ship Collisions
B: FSRU Model
C: Tanker Collision
D: Container Ship Collision
E: Collision Animations – SSI – not included as an appendix to Cabrillo Port Appendix C3, Independent Risk Assessment

Cabrillo Port LNG FSRU Ship Collision Analysis

Draft Report

Revision No.	Date Issued	Status	Developed By	Checked By
A	27 October 2004	Draft Report Issued to Client for Comment	RES/FW	FJP
B	6 October 2004	Draft Report with Client Comments Included	RES/FW	FJP
C	12 November 2004	Final Report with Client Comments Included	RES/FW	FJP

Prepared for:
A J Wolford and Associates
3218 Quiet Lake Drive
Katy, Texas 77450-5721

Prepared by:
Energo Engineering, Inc.
3100 Wilcrest Drive, Suite 240
Houston, Texas 77042

Energo Engineering Project No.: E04116

Energo

[redacted]

TABLE OF CONTENTS

EXECUTIVE SUMMARY ii
1.0 INTRODUCTION 1
1.1 Background 1
1.2 Study Objectives 3
1.3 Project Contract 3
2.0 TECHNICAL APPROACH 4
2.1 Ship-to-Ship Collision Analysis Approaches 4
2.2 Study Approach 5
2.3 Key Assumptions 7
3.0 FSRU COMPUTER MODEL 9
3.1 General Characteristics of the FSRU 9
3.2 FSRU FEM Model 12
4.0 TANKER MODEL 15
4.1 Model Description 15
4.2 Collision Results 18
5.0 CONTAINER SHIP MODEL 22
5.1 Model Description 22
5.2 Collision Results 25
6.0 RESULTS AND CONCLUSIONS 29
6.1 Results Summary and Discussion 29
6.2 Comparison of Tanker and Container Ship Collisions 30
7.0 REFERENCES 34

APPENDIX A ..... PAPER ON NUMERICAL SIMULATION OF SHIP COLLISIONS
APPENDIX B ..... FSRU MODEL
APPENDIX C ..... TANKER COLLISION
APPENDIX D ..... CONTAINER SHIP COLLISION
APPENDIX E ..... COLLISION ANIMATIONS

EXECUTIVE SUMMARY

Background

BHP is considering a Liquefied Natural Gas (LNG) Floating Storage and Regasification Unit (FSRU) to be located offshore Southern California. It is a MOSS-type design that stores the LNG in three spherical aluminum alloy tanks.

One of the risk concerns for the FSRU is collision from another vessel that may breach the LNG containment sphere and release LNG. A separate study has indicted that two ships of concern for collision are a [redacted] (GWT) Oil Tanker and [redacted] GT Container Ship [Ref. 1].

This document describes the results of a detailed collision assessment of the FSRU being impacted by the Oil Tanker and the Container Ship. The assessment is a much improved approach compared to typical "empirical" ship collision assessments in that it accounts for the specific geometry and strength of the FSRU in the collision zone and the bow of the colliding ship via the use of advanced structural finite element method (FEM) analysis. The work scope involved FEM modeling of the FSRU, Tanker and Container Ship in the regions of impact, running of the collision analyses, and the development of a draft and final written report documenting the work.

The results from this work, particularly the hole size and associated collision speed, will be used for the assessment work also being conducted for this project [Ref. 1].

Approach

Specific collision scenarios were evaluated for the Tanker and Container Ship. The collisions were assumed to be 90 degree "T-bone" impact directly into the amidships of the FSRU at the centerline of the middle LNG containment sphere. This is assumed to be the worst case collision angle. The used FEM to account for the "internal" energy dissipation as a result of the crushing of the colliding ship's bow and the FSRU ship structure at the collision interface. The FEM work has been used on several previous ship collision studies and has been benchmarked against laboratory tests. The "external" energy dissipation as a result of the FSRU global response to the collision was also accounted for in terms of rigid motions of the FSRU when it is hit by the colliding ships. The FEM model for the FSRU used in the collision analyses is shown in Figure E.1

Figure E.1 - FSRU FEM Model

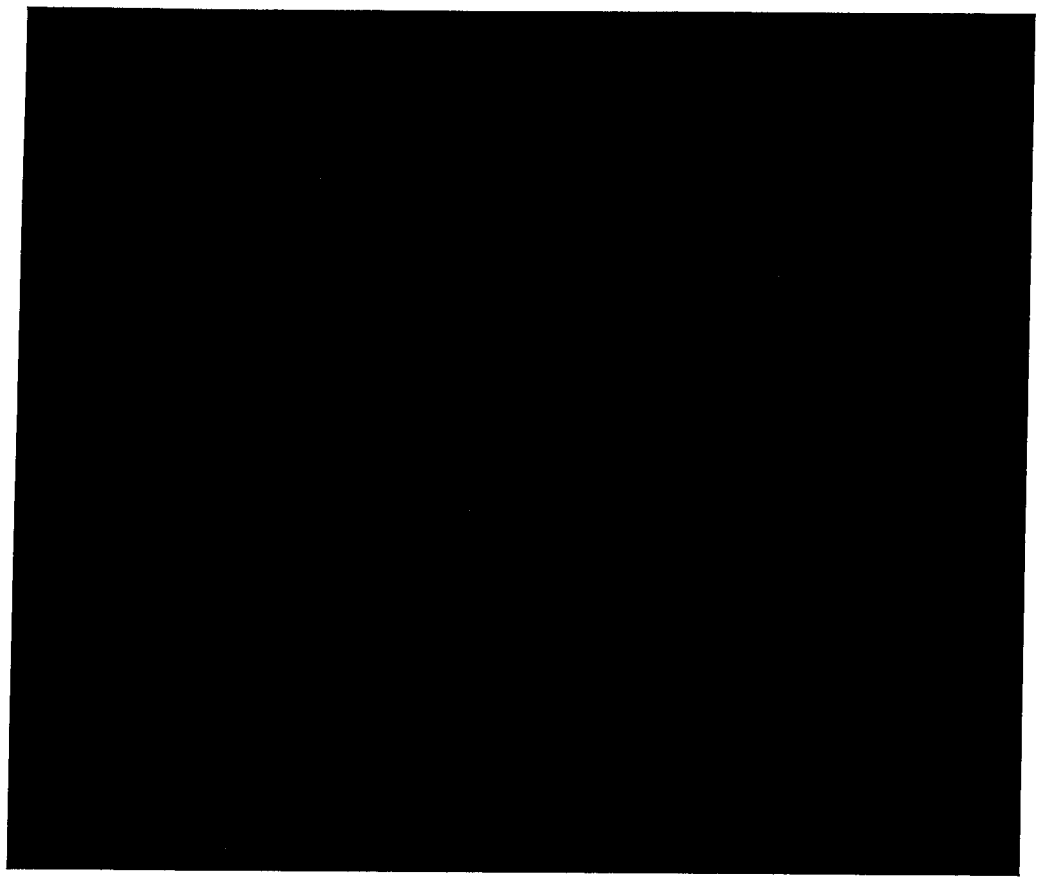

Figure E.2 shows sequential images of the Tanker collision into the FSRU and Figure E.2 shows the collision for the Tanker Ship. In both cases the sequence of failure is similar. The initial contact occurs at the main deck of the colliding ships and then the bulbous section comes in contact with the outer shell of the FSRU. As the colliding ship is driven into the FSRU structure, it ruptures the outer and eventually the inner hull shells (See Image B). The bulbous section of the bow remains within the lower hopper region of the FSRU hull. As the bow structure continues this path, the stem of the colliding ship (upper region of the bow) comes in contact with the LNG sphere skirt structure. This contact then results in large deformations of sphere skirt which in turn deforms the sphere. This ultimately results in rupture of the sphere along the sphere-to-skirt connection (See Image C). Further deformation of the sphere and support skirt occurs as the bow is driven into the FSRU hull structure (Image D).

Figure E.2 - Tanker Collision

[redacted]

Figure E.3 - Container Ship Collision

[redacted]

The resulting collision speeds for each ship that are required to create a hole in the LNG containment sphere are shown in Figure E.4. The dashed lines represent the expected continuation of hole size beyond the finite element analysis work performed here.

Figure E.4 - Collision Speed Versus FSRU Sphere Hole Size

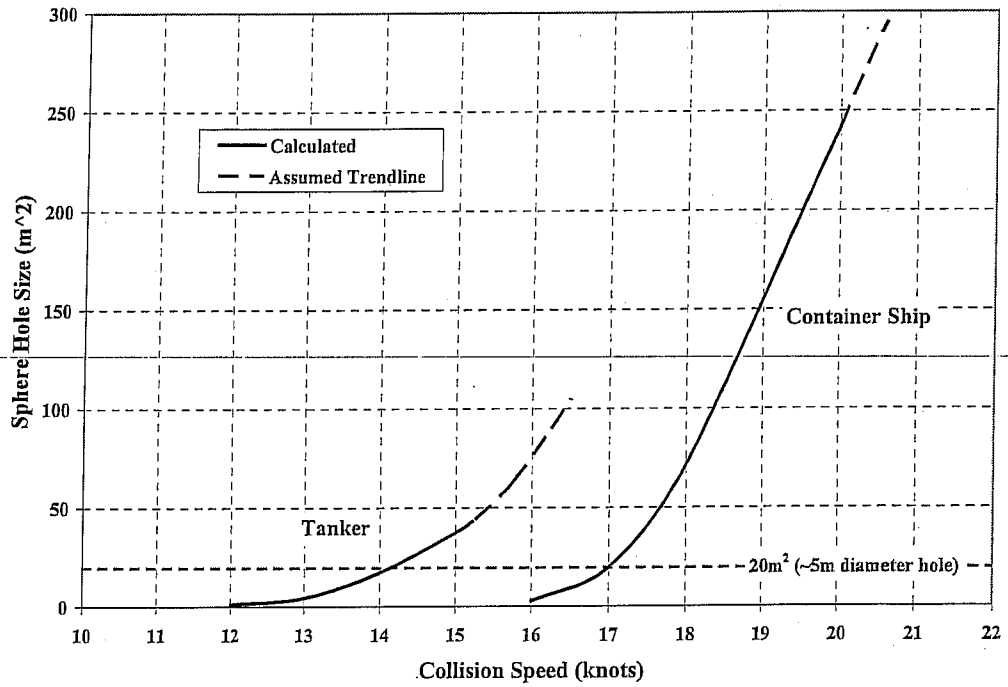

The hole in the LNG sphere is created as the colliding ship penetrates the outer and inner hull shells [redacted] The hole sizes shown in Figure E.4 were based upon a "snapshot" of the hole at the noted impact speed. In reality it is difficult to accurately model the rapid change in the size of a hole [redacted] Instead, it is recommended to interpret the results as two types of holes for this type of failure. The first hole would be "small" up to about 20 square meters (equivalent to a 5 meter diameter circular hole) that would occur for speeds between 12-14 knots for the Tanker and between 16 to 17 knots for the Container Ship. After this, the hole [redacted] may expose a large portion of the LNG sphere, [redacted] In this case the hole should be considered very large and would occur at collision speeds of more than 14 knots for the Tanker and more than 17 knots for the Container Ship.

1.0 INTRODUCTION

1.1 Background

BHP is considering a Liquefied Natural Gas (LNG) Floating Storage and Regasification Unit (FSRU) to be located offshore Southern California. The FSRU will receive LNG from LNG Carriers moored alongside, store the LNG on-board, and then regasify the LNG to gas for transport to shore via pipeline. It is a MOSS-type design that stores the LNG in three spherical aluminum alloy tanks. The FSRU is 286 meters long (938 ft), 65 meters (213 ft) wide and has a displacement of 190,000 DWT displacement. It will be moored in approximately 884 meters (2900 ft) of water using an external mooring turret located at the bow. Thrusters will be used to assist the FSRU in positioning during loading of the LNG. Figure 1.1 shows a schematic representation of the FSRU.

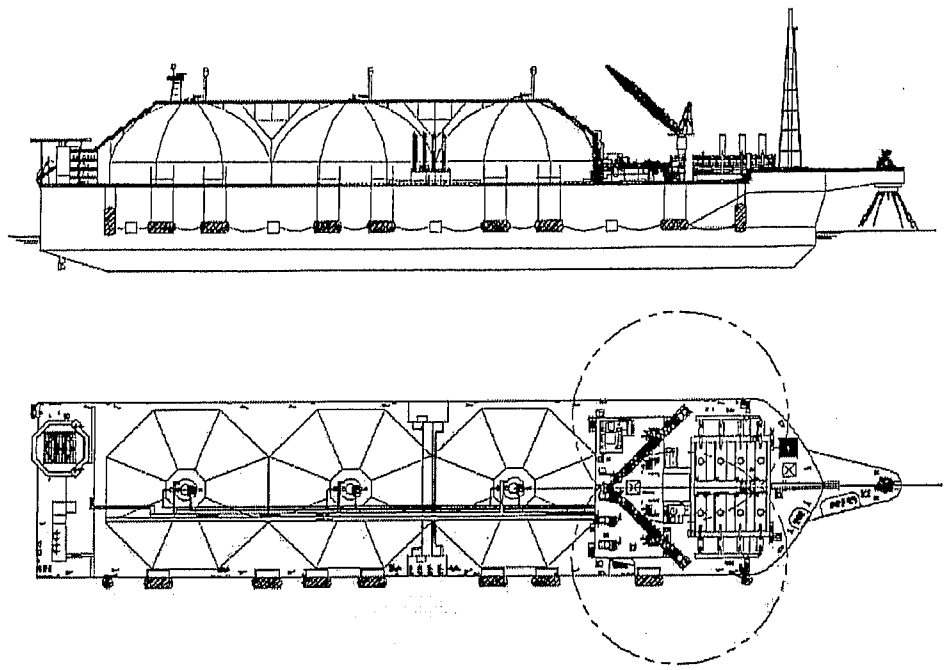

Figure 1.1 - Proposed Cabrillo Point LNG FSRU

Figure 1.2 shows a cross-section view of the FRSU at amidships, including one of the LNG containment tanks.

One of the risk concerns for the FSRU is collision from another vessel that may breach the LNG containment sphere and release LNG. A separate study has indicted that two ships of concern for collision are a [redacted] gross tonnage (GWT) Oil Tanker and [redacted] GT Container Ship [Ref. 1].

This document describes the results of a detailed collision assessment of the FSRU being impacted by the Oil Tanker and the Container Ship. The assessment is a much improved approach compared to typical "empirical" ship collision assessments in that it accounts for the specific geometry and strength of the FSRU in the collision zone and the bow of the colliding ship via the use of advanced structural FEM. The work scope involved FEM modeling of the FSRU, Tanker and Container Ship in the regions of impact, running of the collision analyses, and the development of a draft and final written report documenting the work.

1.2 Study Objectives

The objectives of the study are to determine the effect of ship collision on the FSRU, with specific focus on the potential release of LNG. This is summarized as follows:

- Determine the estimated damage to the FSRU due to a collision of a Tanker and a Container Ship into the FSRU.
- Determine the hole size in the LNG containment, if any, as a function of speed for the colliding Tanker and Container Ship

The results from this work, particularly the hole size and associated collision speed, will be used for the independent risk assessment work also being conducted for this project [Ref. 1].

1.3 Project Contract

The work was performed under contract to and under the direction of A. J. Wolford and Associates, Houston, Texas. This study is part of the independent environmental impact study that is being conducted for the Cabrillo Port LNG FSRU.

2.0 TECHNICAL APPROACH

2.1 Ship-to-Ship Collisions Analysis Approaches

This section briefly describes some of the available methods currently used to simulate ship-to-ship collisions. The section also describes the method used as part of this study and the basis for using this method.

Ship-to-ship collisions represent very complex structural and mechanic interactions, and the degree of damage both to the striking and stuck vessel can vary significantly due to an assortment of variables. Some of the variables influencing damage include striking vessel bow profile and stiffness, struck vessel structural arrangement (e.g., frame spacing, bulkhead/containment barriers, etc.) which relate to the internal mechanics, plus vessel mass and speed which related to the external mechanics, including the "added mass" of water that moves with the vessels.

The ship collision internal mechanics is extremely complex and involve large deformation, deep collapse, fracture and friction between two complex geometries. Over the years different approaches have been developed, from the simplified to the complex. Many of the more complex analytical methods have evolved recently [Ref. 2–7] These advances have been driven by rapid advances in the computer technology and powerful special-purpose FEM packages. In general, there are four possible methods that can be used to evaluate the internal collision mechanics [Ref. 8]. These methods include:

1. *Simple formula* – Methods generally calculate the energy absorption of a ship using generic empirical formulations providing a quick estimation of global structural performance.
2. *Simplified analytical methods* – Methods tend to be more detailed with regards to individual structural components capturing some of the characteristics of the damage process and employing theoretical formulae for structural components.
3. *Simplified finite element methods* – Methods incorporate the use of coarse mesh or super-elements to reduce computational time compared with non-linear FEM simulation. Methods combine the advantages of analytical models for components and conventional finite element approach. [Ref. 9&10].
4. *Non-linear finite element modeling (FEM) simulations* – Methods utilize special-purpose commercial FEM packages, which account for large deformation, contact, non-linear material properties and rupture.

Selection of the most appropriate method is dependent on the specific results that are desired. For this evaluation, the results are intended to provide information on potential consequences related to ship-to-FSRU facility collisions. Specifically, the objectives are to determine the potential damage to the FSRU LNG spheres (e.g., deformation, rupture or hole size) from two different types of striking vessels.

Since the objectives of the collision study are to provide such detail, including the failure mode, associated sphere hole size and ability to accurately distinguish between the structural response of two different types of striking vessels and the LNG terminal arrangement, the more rigorous methodology (i.e., type 4 method listed above) is used. This type of modeling provides the required detail to account for the local behavior of the FSRU hull and sphere structure (i.e., fracturing, large deflection, etc.) and it's very unique arrangement (e.g., large depth, overall hull profile, sphere and support skirt).

The more simplified methods as well as the simplified FEM methods (type 3 method listed above) generally do not account for this level of detail and local effects. In some cases, the more simplified methods can require considerable amount of benchmarking to confirm results. Furthermore, for the FEM approach, some benchmarking related to ship-to-ship collision simulations has been published [Ref. 11]. This material compares laboratory tests results to non-linear finite element analysis results and provides guidance on appropriate modeling parameters methods. A draft of this paper is provided in Appendix A.

2.2 Study Approach

This section outlines the study approach and methodologies used to evaluate the structural resistance of the FSRU to collisions and the relationship to speeds of vessels operating in vicinity.

For the evaluation of ship-to-ship collisions, it is important to understand the complex mechanics that occur during the event. Specifically, there are two distinct parts of the collision event. These include the internal collision mechanics and the external collision mechanics. The definitions are as follows [Ref. 3]:

- *Internal Collision Mechanics* – This involves the structural failure response of the involved ships (e.g., bow of striking vessel and side shell of struck vessel). Analysis of the internal mechanics can be used to obtain the absorbed energy for the ship structure interaction.
- *External Collision Mechanics* – This involves the evaluation of the time dependent rigid body motion of the involved ships accounting for the collision forces and effects of the surrounding water. By analyzing the external mechanics, the total initial kinetic energy that must be absorbed during the ship structural interaction can be computed.

In summary, the internal mechanics relate to the energy absorption of the two colliding vessels while the external mechanics relate to the rigid body motion (e.g., speed) of the vessels. Figure 2.1 shows the overall process in flowchart form.

Figure 2.1 – Approach Methodology

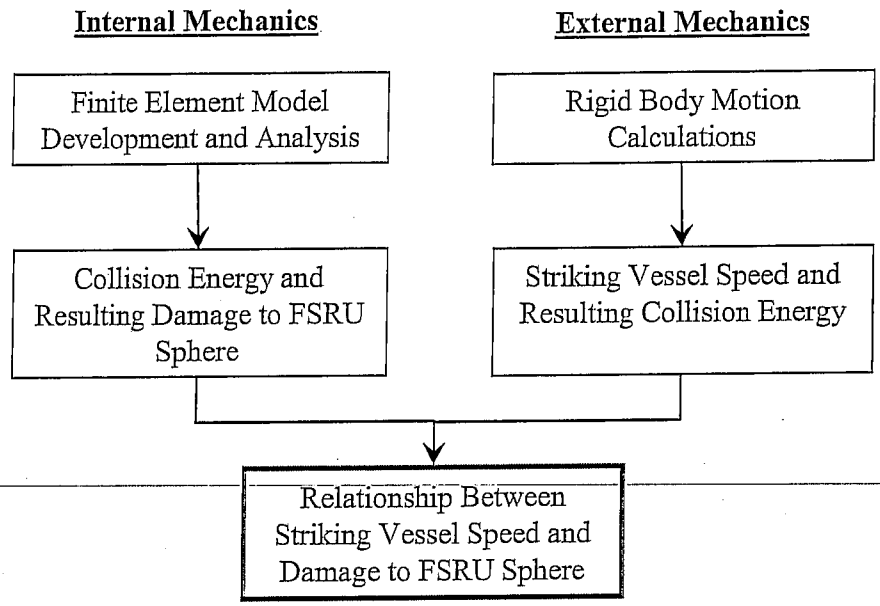

Since the objective of these study is to determine the resistance of the FSRU to ship collisions and relate this to ship striking speeds, breaking the problem up into two distinct parts (i.e., internal mechanics and external mechanics) allows both the structural resistance to be determined as well as the associated speed of the striking vessel. Hence for this study the determination of collision speeds for predicting hole sizes is broken into two mechanics into two distinct parts. The internal mechanics are analyzed by using detailed FEM analysis to determine the energy absorption of the two structures. These results are then used in the external mechanics analysis to determine the speeds of the striking vessel.

Approaching the overall collision study in these two distinct parts is a very efficient way to generate both the structural response (i.e., damage) of the colliding ships as well as the estimated collision speeds of the striking vessels.

2.2.1 Internal Mechanics Evaluation

Using typical structural arrangements, representative sections of the FSRU in way of the center sphere and representative striking vessel bow sections are modeled in detail in the FEM program. The analysis is conducted using LS-DYNA3D™. LS-DYNA™ is a general-purpose, explicit and implicit finite element program used to analyze the nonlinear dynamic response of three-dimensional inelastic structures. The program has fully automated contact analysis capability and error-checking features. Model development is conducted in the ANSYS™ preprocessor. The models are developed in appropriate detail to ensure adequate behavior of the structural elements.

Contact between the striking vessel bow and the target area of the FSRU hull is represented by contact surfaces. The models are used to determine the absorbed energy and the resulting damage to the structures. This is done in the FEA program by pushing the striking vessel bow at a constant velocity into the side shell of the FSRU model.

2.2.2 External Mechanics (Collision Speed Determination)

Using the structural evaluation (i.e., internal mechanic results), the next step is to relate the absorbed energy (i.e., energy versus penetration) with the striking vessel speed. This is accomplished by using external mechanics or rigid body motion calculations. Simplified classical theory for the analysis of external collision mechanics [Ref. 8] are used to determine the strike vessel speed for the calculated absorbed collision energies using the appropriate vessel mass and added-mass coefficients.

The ship-to-ship collision external mechanics relates to the energy lost (or released) during the impact of two moving ships. When two moving bodies collide, a portion of the total kinetic energy is generally lost during collision, except in the case of purely elastic impact. Typically in ship-to-ship collision analysis, purely plastic impact is assumed (i.e., no re-bounding between the two ships). In such cases, the total kinetic energy after collision will be smaller than before the collision (i.e., energy is lost during the collision event).

The kinetic energy lost during collision has to be absorbed by the deformation/tearing of the ship structure. The deformation energy is calculated via FEA (describe above in the Internal Mechanics section). By equating the lost kinetic energy from external collision mechanics to the deformation energy from internal collision mechanics, the relationship between the ships collision speed and the resulting damage to the FSRU can be determined.

The external mechanics calculations used in this project follows the formulations as published in the research paper "On Impact Mechanics in Ship Collisions" [Ref. 12]. The formulations are conducted using MathCAD worksheets.

2.3 Key Assumptions

Several key assumptions had to be made during the study due to the limited timeframe and funding available. These are described below.

- *Collisions Conducted for Two Ships Only.* There are numerous types of ships that pass the FSRU on a regular basis, of different size and speed. Only two ships were modeled for this study – the tanker and container ship. Results may be different for other ships of other service and sizes (e.g. cruise ship).

- *Single Bow Configurations.* The ship bows used in the analysis are typical for the types of these ships that operate in the region. Other tanker and container ships of the same size, but with different bow geometry and strength may produce different results, although the results here are felt to be representative.

- *Single Collision Case for Each Ship.* All of the impacts were assumed to be a 90 degree (or "T-bone") collision of the ships into the FSRU at the centerline of the FSRU middle tank. This is assumed to be the worst case scenario for such collisions.

- *Fully Laden Ships.* The colliding ships were assumed to be fully laden (full of oil or containers) representing a single draft condition. The draft may vary from 15 to 20 meters depending upon the cargo on board, for example, water ballast in lieu of oil. This would result in a change in the geometry of the FRSU and colliding ship interface and may change the collision results. It would also change the mass of the colliding vessel (hence collision energy).

- *Energy Absorption for a Turret Moored FSRU.* As noted later, the collision work accounts for internal and external mechanics of the collision. The external mechanics is associated with the energy absorption of the turret moored FSRU during the collision. For the purposes of this study, it was assumed that this can be represented as somewhere in between a fixed and free floating condition (an average of both) was used. This is estimated to be conservative (i.e., higher impact speed to create a hole), since a turret mooring is more likely close to a free floating condition. A more exact energy absorption capability of the turret moored FSRU would have to be determined in a special study.

- *Effect of Compressing LNG in the Containment Sphere During a Collision.* Once the colliding ship begins to push inward on the containment sphere, the LNG liquid will force an outward pressure and may help to "burst" the sphere in the region of contact. This has been captured by placing a small outward pressure on the sphere that induces failure quicker than just a hollow sphere. However, this effect needs to be studied further.

- *Sloshing.* The spherical LNG tank was considered to be near full when the collision occurs in order to maximize the release quantity. A full tank has minimal sloshing since there is minimal free surface area. If the tank were partially full at the time of collision, then the impulse force of the collision will cause the LNG liquid to slosh, and this may create large hydrodynamic impulse loads on the tank sidewalls, perhaps increasing damage to the tank in the region of the collision. This issue would have to be determined in a separate study that includes the effects of sloshing.

3.0 FSRU COMPUTER MODEL

3.1 General Characteristics of the FSRU

The FSRU is similar in design to seagoing LNG MOSS carriers with the LNG cargo contained in spherical tanks that are located along the centerline of the vessel.

Table 3.1 –FRSU Particulars

Description	Values
Length	286 m (938 ft)
Breath	65 m (213 ft)
Depth	31 m (102 ft)
Approximate Design Draft (laden)	13.2 m (43 ft)
Deadweight Tonnage	150,000 tonnes
Laden Displacement	190,000 tonnes

The collisions were assumed to occur at approximately amidships, at the centerline of the middle LNG spherical tank. The cross section of the ship in this region is shown schematically in Figure 3.1. This region is believed to represent the worst case for collision related to LNG release for several reasons. First, it provides the shortest distance between the outer hull (side shell) and the LNG sphere. As shown later via the FEA analysis, the distance the colliding ship has to crush into the FSRU in order to get to the containment is critical in terms of energy dissipation. The shorter the distance, the more likely that there will be a penetration of the LNG containment. Second, the side shell in this region is not directly supported at the deck level due to the hole for the spherical tank. Instead, it is supported to the bow and aft directions only by transverse bulkheads. This support arrangement differs from the bow and aft tanks since they are supported on at least one side by the deck structure, which creates an overall stronger structural support system. Hence the center tank appears to be the "weakest" point along the ship in terms of ship collision and was therefore selected as the location for the ship impacts.

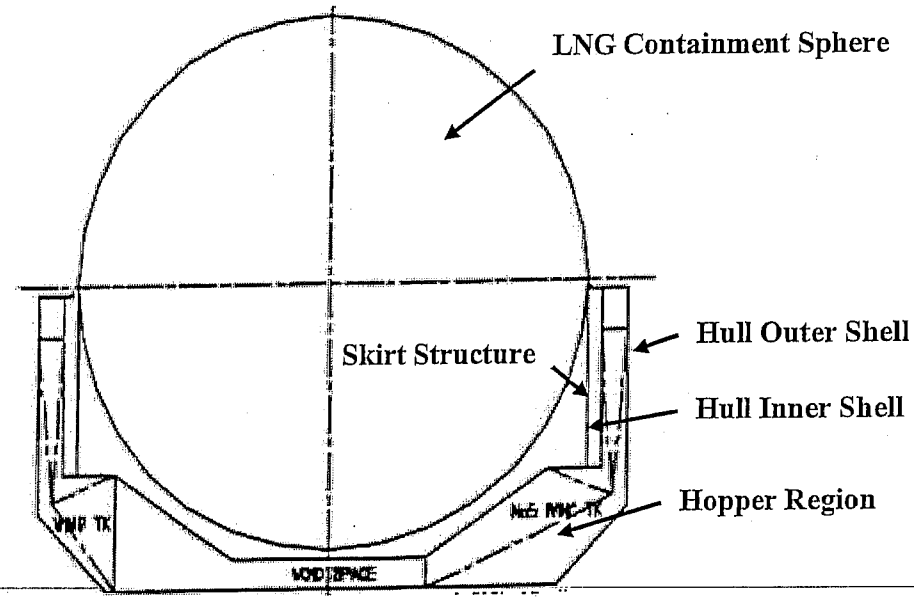

Figure 3.1 - Cross Section of FSRU at Amidships

Even though this is the region of greatest collision concern, the structural arrangements of the FSRU present a formidable four-layer barrier to ship collision. A colliding ship would have to first penetrate the hull outer shell, then the hull inner shell, then the skirt structure that supports the containment sphere, then the containment sphere itself. Table 3.2 summarizes the key properties of these ship structure components which must all be breached in order to allow an LNG release. These barriers are important because as seen later in the collision analyses, this is the contact region of the colliding ship's bow fore-peak.

Table 3.2 –FRSU Barriers

Component	Distance from Outer Shell (m)	Material	Plate Thickness (mm)	Stiffening
Hull Outer Shell	0	Normal Strength Steel	13.5 - 45	Web frame spacing = 3.7 m Longitudinal stiffener spacing = 0.85m
Hull Inner Shell	3	Normal Strength Steel	13.5 - 45	Web frame spacing = 3.7 m Longitudinal stiffener spacing = 0.85m
Skirt Structure	4.5	High Strength Steel	65 max.	Ring stiffener spacing = 3.0 m Vertical stiffeners = 1.2 m
Sphere	4.5+	Aluminum Alloy	65 max.	None

In addition to the vertical structural components described above, the hopper region of the FSRU also provides a formidable barrier to collision. This region is heavily reinforced in order to provide the foundation for the skirt structure which supports the spherical tank. Note that the tank is connected to the skirt at the tank "equator," with the skirt carrying the spherical tank loads into the vessel the skirt bottom located in the hopper area. This is the only structural connection of the sphere to the ship structure. The considerable strength of the hopper area is important for collisions as seen later in the collision analyses, since this is the contact region of the colliding ship's bulbous bow.

Another important factor for ship collisions is the height of the double hull composed of the outer and inner shell (called sideshell here). This is because for some ship collisions, the colliding ship fore-peak may be at a height that is above the top height of the sideshell of the ship that is struck. In this case, the fore-peak of the colliding ship may extend over the top of the struck ship sideshell, causing damage to components on the deck. Figure 3.2 shows an example of this type of collision. If the struck ship was a MOSS-type LNG carrier with spherical tanks that protrude above the deck, it may be possible for the colliding ship forepeak to breach a hole in the spherical tank above the deck level. However, for the LNG FSRU evaluated in this study, the sideshell top is exceptionally high, approximately 5 meters (16 ft) higher than the typical tanker used in this study. This higher sideshell provides added protection to prevent this type of damage. This is confirmed later in the ship collisions where all of the impact damage occurs below the deck level.

Figure 3.2 - Example Damage to a Colliding Ship Bow in the Case where the Stuck Ship had a Low Sideshell Top Elevation

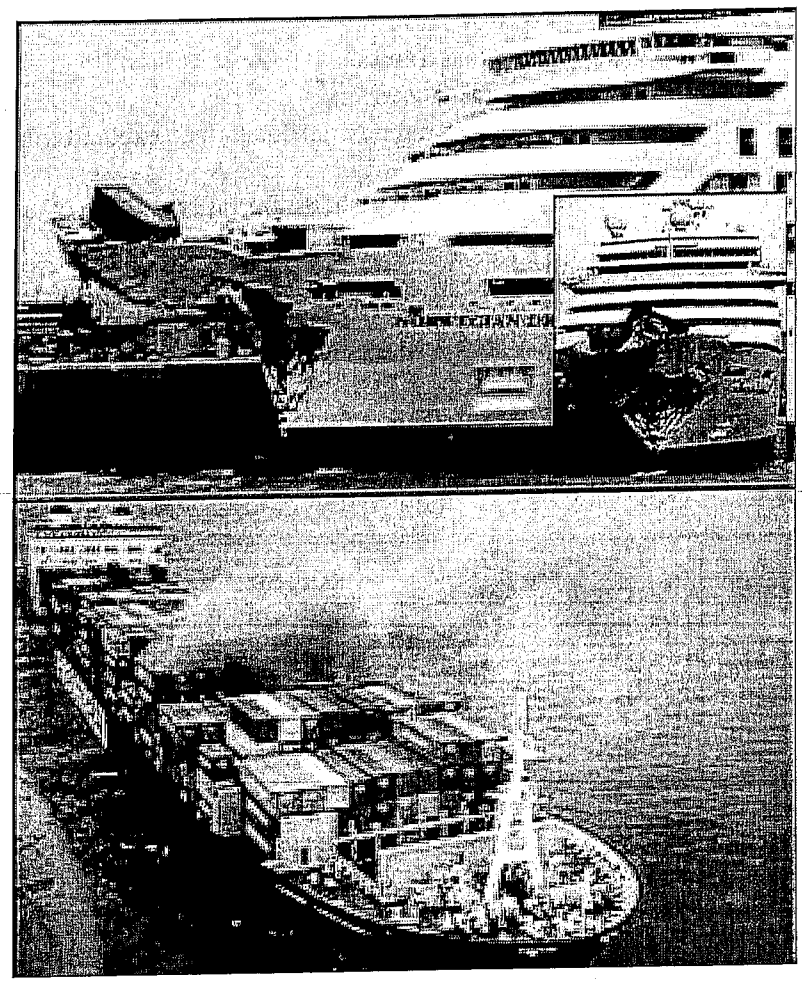

3.2 FSRU FEM Model

As previously noted, it is only necessary to model the FSRU in detail in the collision areas, this case being amidships. A more complete model of the FSRU can be constructed, but this would take additional modeling and analysis effort and would not improve results for the purposes of this study. Therefore, the FEA modeling efforts were focused on the ship structural details in this region.

Figure 3.3 shows a general view of the resulting FEA model of the FRSU. This model was used for both the Tanker and Container Ship collision analysis. The colors shown in the figure represent different plate property types (i.e., different plate thicknesses). The model was based upon the structural design drawings of the FSRU as contained in

Reference 13 as well as additional structural drawing information provided by BHP [Ref. 14]. Key structural features were modeled explicitly as follows:

- Side and inner shells are modeled explicitly
- All transverse bulkheads, girders, and frames
- All longitudinal bulkheads, decks, and stringers
- Longitudinal stiffeners at the contact regions (stiffeners not explicitly modeled were smeared into adjacent steel plates)
- Detailed modeling of hopper region (area where the bulbous bow of colliding ship comes in contact)
- High strength skirt tank support
- Aluminum LNG tank
- Material strength properties per design specifications

Material properties for the FSRU are shown in Table 3.3.

Table 3.3 – Material Properties of LNG FSRU Structural Components

Steel Grade	Yield Strength (N/mm^2)	Ultimate Strength (N/mm^2)	Rupture Strain	Young's Modulus (N/mm^2)	Poisson Ratio
Mild Steel	235	460	0.22	200000	0.3
Skirt EH36	355	555	0.21	200000	0.3
Tank Sphere AL 5083	125	275	0.09	70,000	0.3

The transverse bulkheads and bottom hull were only modeled to the FSRU centerline due to symmetry. However the spherical tank and high strength skirt tank support were modeled in full in order to more accurately capture the failure mode of the sphere-skirt system. It was felt that a symmetric boundary condition may not be accurate, especially for the sphere, and therefore these components were modeled completely in order to avoid this concern.

The outer shell, inner shell, skirt structure, sphere and hopper area all have a finer grid mesh in the region of collision contact in order to more accurately capture local structural failures at the collision interface. These can be seen via close examination of Figure 3.3.

Appendix B contains additional information on the FSRU FE model.

Figure 3.3 – FSRU Finite Element Model

[redacted]

4.0 TANKER COLLISION

4.1 Model Description

Based on the quantitative risk assessment (QRA) data collection on traffic in the vicinity of the proposed LNG terminal (Ref. 1), the most probable tanker passing the terminal will be a very large crude carrier (VLCC) approximately [redacted] deadweight tonnage (DWT). This size vessel represents the smaller range of VLCC's which range in size between 200,000 and 320,000 DWT. Representative particulars for this type of vessel are presented in Table 4.1. It is important to note that these are approximate values and not intended to represent one particular vessel but instead representation of the most probable tanker in vicinity of terminal.

Table 4.1 – Representative VLCC Particulars

[redacted]

Based on these parameters a finite element model (FEM) was developed using available information on representative tankers of this general size. Since the focus of the study is the collision resistance of the LNG terminal, only the bow section of the striking vessel is modeled in detail. This generally includes the bow structure up to the first transverse bulkhead forward of the cargo block. In this region the main structural members are model to represent the typical scantlings of these types of vessels and most importantly their typical approximate stiffness and shape characteristics.

Figure 4.1 shows the profile and the cut section of the VLCC tanker model. The cut section shows the interior detail such as framing, bulkhead and decks. The colors shown in the Figure 4.1 represents different plate property types (i.e., different plate thicknesses). The material properties used in the model are shown in Table 4.2.

Table 4.2 – Material Properties of Tanker Structural Components

Steel Grade	Yield Strength (N/mm^2)	Ultimate Strength (N/mm^2)	Rupture Strain	Young's Modulus (N/mm^2)	Poisson Ratio
AH 32	315	515	0.22	200000	0.3
Mild Steel	235	460	0.22	200000	0.3

The parameters shown in Table 4.1, specifically the general dimensions and laden displacement (mass), are also used to determine the collision kinetic energy for various tanker speeds. It is important to note that the laden displacement and draft are assumed. The laden case represents the maximum kinetic energy that can be produced by the tanker.

Figure 4.1 – Representative Tanker FEM

[redacted]

4.2 Collision Results

This section summarizes the finite element analysis (internal mechanics) and the associated collision speed (external mechanics) results. Descriptions and images of the structural response are presented as well as the estimated vessel collision speeds required to cause specific damage levels.

Images of the tanker collision simulation are shown in Figure 4.2. For this case, the initial contact occurs at the main deck of the tanker and then the bulbous section comes in contact with the outer shell of the FSRU. As the tanker is driven into the FSRU structure rupture of the outer and eventually the inner hull shells occurs in way of the container ship main deck (See Image B). The bulbous section of the bow crushes at the lower hopper region of the FSRU and does not breach the sphereical tank. As the bow structure continues this path, the stem of the tanker (upper region of the bow) comes in contact with the LNG sphere skirt structure. This contact then results in large deformations of sphere skirt which in turn deforms the sphere. This ultimately results in rupture of the sphere in way of the sphere-to-skirt connection (See Image C). Further deformation of the sphere and support skirt occurs as the bow is driven into the FSRU hull structure (Image D).

Figure 4.3 presents snap shots of the sphere deformation and rupture behavior from the tanker collision. The location of the skirt relative to the sphere structure is noted on the images. Note that initial failure occurs at this region and expands outward around the circumference above the skirt.

Figure 4.2 – Tanker Collision

[redacted]

Figure 4.3 – Sphere Rupture Behavior from Tanker Collision

[redacted]

Figure 4.4 shows the calculated relationship between estimated FSRU sphere hole size and the tanker collision speeds.

Figure 4.4 – Tanker Collision Speed Versus FSRU Sphere Hole Size

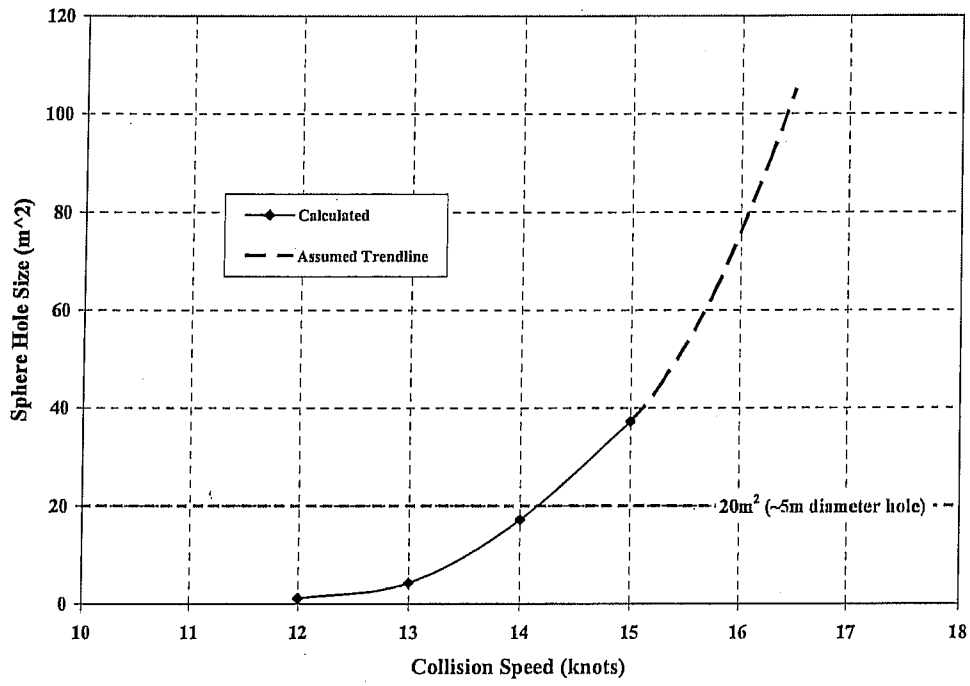

Section 6.2 provides additional discussion of the collision results.

5.0 CONTAINER SHIP COLLISION

5.1 Model Description

Similar to the tanker model, a representative container ship was selected based on QRA data collection on traffic in the vicinity of the proposed LNG terminal. Based on this work, the most probable container ship passing the terminal will be in the range of [redacted] gross tonnage (GWT). This represents a moderate to large container ship with a twenty feet equivalent unit (TEU) capacity of 4,000 to 5,000. TEU relates to the number of containers the vessel can carry. For comparison purposes, the latest generation of large container ships has capacities between 7,000 to 8,000 TEU.

Representative particulars for the container ship used in this study are presented in Table 5.1. It is important to note that these are approximate values and not intended to represent one particular vessel but instead representation of the most probable tanker in vicinity of terminal.

Table 5.1 – Representative Container Ship Particulars

[redacted]

Similar to the tanker model development, available information on representative container ships of this general size was used to develop the FEM of the bow structure. The bow structural model includes the typical scantlings and provides the approximate stiffness and shape characteristics found for this size and type of vessel. The parameters shown in Table 5.1 are also used to determine the collision kinetic energy for various container speeds. The material properties used in the model are shown in Table 5.2.

Table 5.2 – Material Properties of Tanker Structural Components

Steel Grade	Yield Strength (N/mm^2)	Ultimate Strength (N/mm^2)	Rupture Strain	Young's Modulus (N/mm^2)	Poisson Ratio
A	235	475	0.22	200000	0.3
AH 36, DH 36	355	555	0.22	200000	0.3

Figure 5.1 shows the profile and the cut section of the container ship model. The cut section shows the interior detail such as framing, bulkhead and decks. The colors shown in the Figure 5.1 represents different plate property types (i.e., different plate thicknesses).

Figure 5.1 – Representative Container Ship FEM

[redacted]

5.2 Collision Results

This section summarizes the finite element analysis (internal mechanics) and the associated collision speed (external mechanics) results. Descriptions and images of the structural response are presented as well as the estimated vessel collision speeds required to cause specific damage levels.

Images of the container collision simulation are shown in Figure 5.2. For this case, the initial contact occurs above the main deck of the container ship and then the bulbous section comes in contact with the outer shell of the terminal. As the container ship is driven into the terminal structure rupture of the outer and eventually the inner hull shells occurs in way of the container ship main deck (See Image B). The bulbous section of the bow crushes at the lower hopper region of the terminal and does not breach the sphereical tank. As the bow structure continues this path, the stem of the container ship (upper region of the bow) comes in contact with the LNG sphere skirt structure, resulting in large deformations of sphere and ultimately rupture of the sphere occurs in way of the sphere-to-skirt connection (See Image C). Further deformation of the sphere and support skirt occurs as the bow is driven into the terminal hull structure (Image D).

Figure 5.3 presents snap shots of the sphere deformation and rupture behavior from the container ship collision. The location of the skirt relative to the sphere structure is noted on the images. Note that initial failure occurs at this region and expands outward around the circumference above the skirt.

Figure 5.2 – Container Ship Collision

[redacted]

Figure 5.3 – Sphere Rupture Behavior

[redacted]

Figure 5.4 shows the calculated relationship between FSRU sphere hole sizes and container ship collision speeds.

Figure 5.4 – Container Ship Collision Speed Versus FSRU Sphere Hole Size

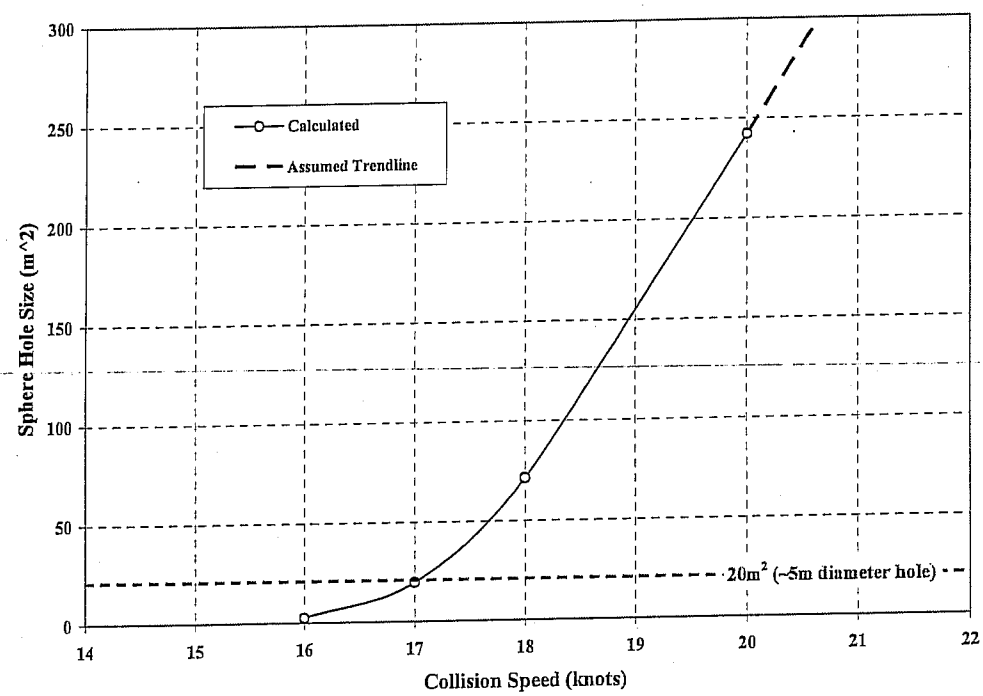

Section 6.2 provides additional discussion of the collision results.

6.0 RESULTS AND CONCLUSIONS

6.1 Results Summary and Discussion

Specific collision scenarios were evaluated for the Tanker and Container Ship. The collisions were assumed to be 90 degree "T-bone" impact directly into the amidships of the FSRU at the centerline of the middle LNG containment sphere. The collisions accounted for the "internal" energy dissipation as a result of the crushing of the colliding ship's bow and the FSRU ship structure at the collision interface via FE analysis. The "external" energy dissipation as a result of the FSRU global response to the collision was also accounted for via purpose-built energy spreadsheets. The resulting collision speeds for each ship that are required to create a hole in the LNG containment sphere are shown in Figure 6.1. The dashed lines represent the expected continuation of hole size

Figure 6.1 - Collision Speed Versus FSRU Sphere Hole Size

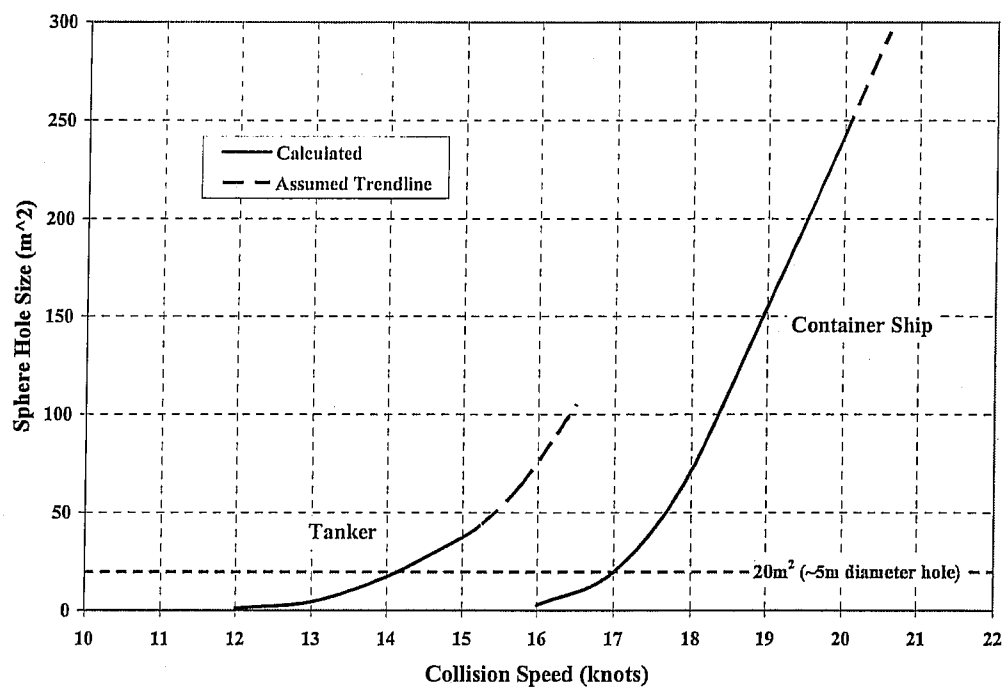

The hole in the LNG sphere is created as the colliding ship penetrates the outer and inner hull shells and then 'pushes" the skirt structure into the sphere. The skirt structure is approximate 60mm (max) of high strength steel and it is difficult for the ship bow to simply "puncture" the skirt. Instead, the bow pushes laterally on the skirt which is attached to the ship structure at the skirt base and at the sphere equator. The result is that the skirt transfers the lateral collision load into these reaction points, especially at the sphere equator. This creates a high strain region along a linear line at the skirt-sphere interface, resulting in an inward pressure on the sphere. The sphere resists this pressure

via local shear of the 60mm (max) thick sphere aluminum alloy as well as hoop stresses. However, these stresses grow rapidly until the sphere "tears" [redacted] – sphere interface. The hole sizes shown in Figure 6.1 were based upon a "snapshot" of the hole at the noted impact speed. In reality it is difficult to accurately model the rapid change in the size of a hole associated with a tear. Instead, it is recommended to interpret the results as two types of holes for this type of failure. The first hole would be "small" up to about 20 square meters (equivalent to a 5 meter diameter circular hole) that would occur for speeds between 12-14 knots for the Tanker and between 16 to 17 knots for the Container Ship. After this, the hole can be quite large with a long tear that may expose a large portion of the LNG sphere, [redacted] In this case, the hole is very "large" and would occur at collision speeds of more than 14 knots for the Tanker and more than 17 knots for the Container Ship.

The collision holes for the LNG FSRU studied here are of different character than may be seen with collisions of other types of vessels such as double hull oil tankers or membrane LNG ships. For these types of ships, the colliding ship literally "punctures" the outer and inner hull shells via the bow fore peak or the bulbous bow. These types of holes tend to be regular shaped for T-bone type collisions, often reflecting the shape of the colliding ship's bow. This needs to be considered if the results of this work are compared to the results of collision analyses for those types of vessels.

The collision speeds required to first create a hole are at first glance quite high for collisions of such large ships. This is due to the design of the LNG FSRU which uses a MOSS type configuration. As previously noted, the MOSS configuration results in four barriers that must be breached prior to the loss of LNG. These are the hull outer shell, the hull inner shell, the skirt structure that supports the containment sphere, and the containment sphere itself. In particular the high strength 60mm (max) thick skirt structure presents a formidable barrier. Another factor is the distance from the hull outer shell to the LNG containment. The further inboard that the colliding ship must travel, the larger the amount of energy that is dissipated in crushing of the FSRU structure and of the colliding ship's bow. For a MOSS type configuration this distance is much larger than other types of double hull ships where the cargo is contained immediately adjacent to the hull inner shell.

6.2 Comparison of Tanker and Container Ship Collisions

Although the Container Ship is considerably smaller than the Tanker, it can also breach the LNG containment at a speed not much greater than the Tanker. There are several factors that account for this. The first is the shape of the bow on each of the ships. Figure 6.2 shows a comparison of the bow profile of the Container Ship and Tanker. The Container Ship is seen to be much more narrow since these ships are built for a higher speed and have a more refined and sleek hydrodynamic profile. In contrast, the Tanker bow profile has a larger and deeper profile. Hence the Container Ship tends to cut through the FSRU structure more efficiently, particularly the outer and inner hull shells. The ship still has sufficient energy by the time that it gets to the formidable skirt structure

to breach the LNG sphere. The Tanker tends to cause a lot of damage to its own bow and the FSRU outer and inner hull shells due to its large contact area at the collision interface. The result is that there has been a lot of energy dissipation by the time the now damaged bow gets to the skirt structure – although it does eventually penetrate the LNG sphere, although it would have to be going at near its top speed prior to the collision. If the Tanker bow were of similar design to the Container Ship it would breach the LNG containment at a much lower speed.

Figure 6.2 - Comparison of Tanker and Container Ship Bow Profiles

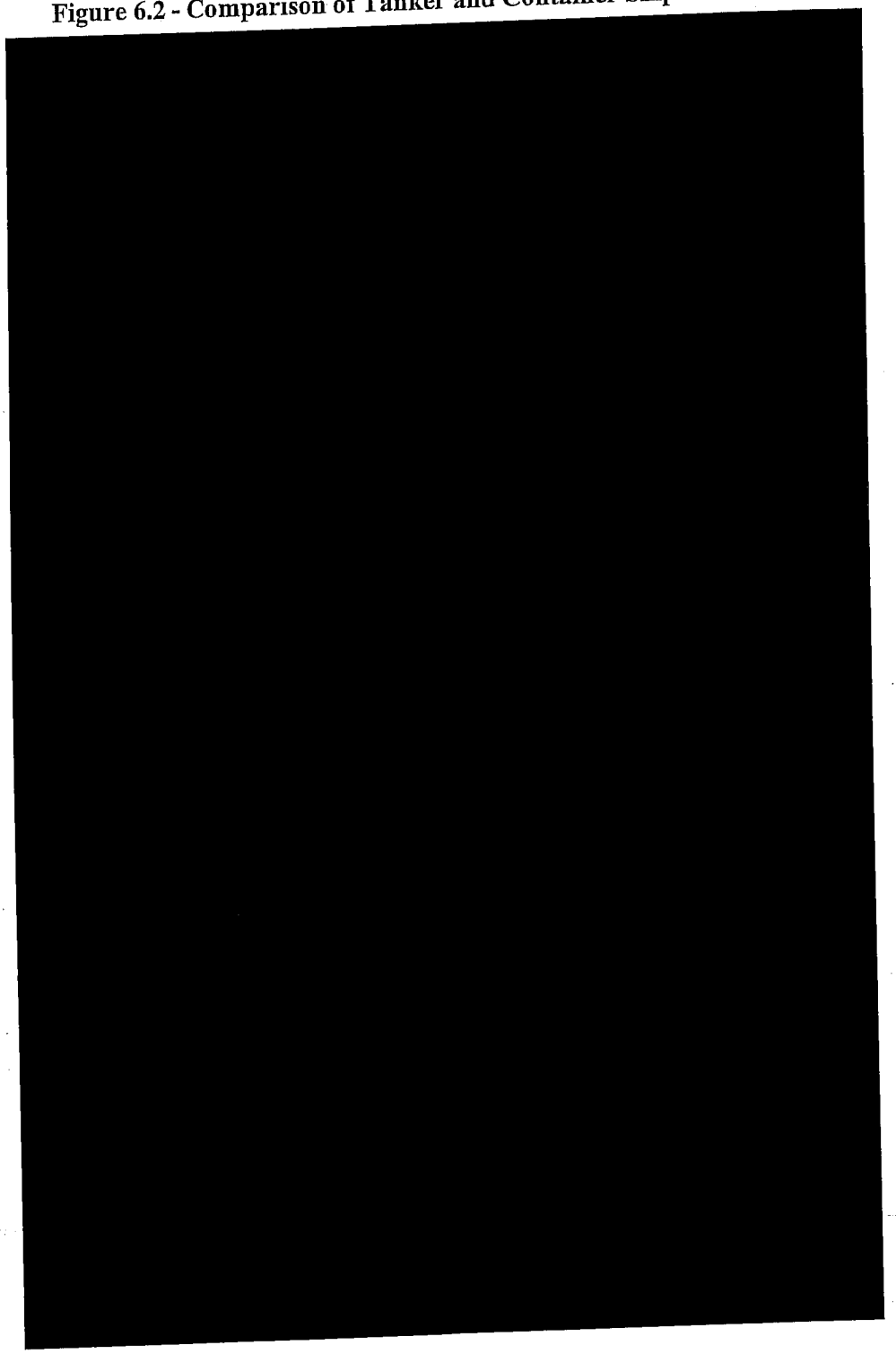

The second effect when comparing the Tanker and Container Ship collisions is the effect of the external energy during the collision that is dissipated by the global motion of the FSRU as it responds to the collision. Table 6.2 shows a comparison of the general size of each of the vessels in terms a weight (or mass equivalent) basis. The Tanker is slightly larger than the FSRU so when it impacts the FSRU, the FSRU is "pushed" in a rigid body manner since the masses are similar. This means that some of the collision energy is dissipated in motion of the FSRU via external energy as it has been called in this study. In comparison, the Container Ship is much smaller than the FSRU so when it impacts the FSRU, there is a much smaller response of the FSRU in terms of global motion and a resulting smaller amount of external energy dissipation. The result is that there is more internal energy that has to be dissipated via crushing of the Container Ship bow and the FSRU ship structure. The net result is that the Container Ship is able to penetrate further into the FSRU.

Table 6.2 - Comparison of Sizes for FSRU, Tanker and Container Ship

7.0 REFERENCES

[1] A.J. Wolford and Associates, "Cabrillo Point LNG Deepwater Port Risk assessment," October 2004.

[2] Simonsen, BC., 1997 Ship grounding on rock: I & II., Marine Structures, 10:519–84.

[3] Paik J.K., Chung J.Y., Choe I.H., Thayamballi A.K., Pedersen P.T., Wang G., 1999. On rational design of double hull tanker structures against collision. SNAME annual meeting, Baltimore MD.

[4] Wang, G., Atita, K., Liu, D., 2000. Behavior of a Double Hull in a Variety of Stranding or Collision Scenarios. Marine Structures, Vol. 13 (2000), pp.147-187.

[5] Brown, A. and Chen, D., 2001. Probabilistic Method for Predicting Ship Collision Damage, Oceanic Engineering International.

[6] Suzuki, K., Ohtsubo, H., Sajit, C., 2000. Evaluation method of absorbed energy in collision of ships with anti-collision structure. Ship Structure Symposium on "Ship Structures for the New Millennium: Supporting Quality in Shipbuilding, Arlington, VA, 13-14 June.

[7] Pedersen, P.T., 2002. Collision risk for offshore structure, Journal of Engineering for the Maritime Environment, Proceedings of the Institution of Mechanical Engineers, 216:M1, 29-44.

[8] Wang G, Spencer J, Chen Y. "Assessment of a ship's performance in accidents," Marine Structures, 2002, pp. 313-333.

[9] Peterson, M.J., "Dynamics of Ship Collisions," Ocean Engineering, Vol. 9, No. 4, 1982, pp. 295-329.

[10] Puskar, F.J. and Litton, R.W. "Ship Collision Analysis for the Kawasaki Island Steel Platforms," OTC Paper 7141, Offshore Technology Conference, May 3-6, 1993, Houston, Texas.

[11] Wu, F., et. al., "Using Numerical Simulation to Analyze Ship Collision," 3rd International Conference on Collision Grounding of Ships, Izu, Japan, October 25-27, 2004.

[12] Pedersen, P.T. and Zhang, S., "On Impact Mechanics in Ship Collisions," Marine Structures, Vol. II, 1998, pp. 429-449.

[13] BHP Billington LNG International, Inc. "Cabrillo Port Application for Deepwater Port License," June, 2003.

[14] BHP, FSRU detailed structural drawings, October 2004.

APPENDIX A

PAPER ON NUMERICAL SIMULATION OF SHIP COLLISIONS

Using Numerical Simulation to Analyze Ship Collision

Fuqiang Wu
Energo Engineering

Robert Spong
Energo Engineering

Ge Wang
American Bureau of Shipping, Corporate Technology

ABSTRACT: Nonlinear finite element method (FEM) is a powerful tool for analyzing ship collision problem and has seen more and more applications in recent years. The reliability of the numerical simulation results largely depends on the proper definition of the problem and careful control of some critical parameters. As part of a benchmarking exercise for a ship-to-ship collision project, the work presented in this paper presents a comparison between FEM numerical results and laboratory test results of a scaled double hull structure representing ship-to-ship collision/grounding scenarios. The general structural responses (i.e., load and energy results) and major failure modes determined from the FEM compared well to the laboratory test. However, some deviations were observed and attributed to specific FEM parameters. These parameters and their associated influence on the FEM simulation results are discussed in detail. The exercise confirms the validation of the numerical simulation technique in application on the ship collision problems and provides insight and guidance into some of the key numerical modeling procedures and controls required in the simulation of these complex structural interaction problems.

1. INTRODUCTION

Of recent, there has been a tremendous drive by industry to meet the present and anticipated future energy demands of many industrial nations. One of these energy initiatives by industry to meet these demands has been in the production and distribution of liquefied natural gas (LNG). Much of the LNG energy initiatives involve development of infrastructure centered on ship-borne transportation coupled with land-based or offshore reception/storage terminals which are typically located within or around existing ports or commercial centers.

With the introduction of these new LNG terminals comes the inevitable question of what are the potential risks related to the new activities in and around these ports and commercial centers. Of particular interest is the risk of ship collisions due to the additional vessel traffic. In order to identify and address these potential risks, industry has sanctioned studies to determine both the potential collision frequencies for various port traffic patterns as well as the related consequences should such an event occur.

During the course of a risk study, collision frequencies were determined, and limitations were recognized in the damage estimates using traditional approaches. The interested parties wanted to have a better understanding of collision resistance accounting for:

- Different striking vessels
- Various collision speed and angles
- Different structural arrangement
- Different failure criteria (i.e., loss of containment, out of service, etc.)

These requirements effectively drove the consequence analysis towards applying detailed finite element analysis (FEA) for calculating structural damage. However, prior to attempting such complex analysis, there was a need to conduct benchmark studies. This need was further reinforced because of the limited publication of mechanical testing and numerical analyses on collision resistance of ship structures.

This paper presents the frame work of this benchmarking exercise used to provide the starting point for a more detailed ship-to-ship collision analysis. The objective of the exercise was to ensure that these detailed simulations capture the structural behavior in a proper manner and provide reliable results. Specifically, the benchmarking exercise set out to accomplish the following:

- Determine appropriate finite element modeling approach
- Determine appropriate values for some of the key analysis variables
- Predict structural resistance (i.e., force vs. penetration)
- Simulate the observed behavior (i.e., tearing, bucking, etc.)

This was done by comparing the FEA results to actual scaled mechanical test results.

2. NUMERICAL SIMULATION APPROACH

The 1990's was characterized by the remarkable advances in analytical solutions of various damage mechanisms in collision and grounding accidents (ISSC 2003). A series of analytical methods was developed and applied (Wierzbicki 1992-1999, Simonsen 1997, Paik et al. 1999, Wang et al. 2000, Brown et al. 2001, Suzuki et al. 2000, Pedersen 2002). These became the main theme of 1990's.

Non-linear finite element model (FEM) simulations are reliable and provide much more detailed information than other approaches. These are especially efficient in representing large bending of local plates, multi-axial stress fields, time-dependent strain hardening and strain rate effects on material properties, etc.

The rapid advances in the computer technology make numerical simulation, a formidable task only a couple of years ago, a viable choice now. Many powerful special-purpose FEM packages, such as DYNA3D, DYTRAN, ABAQUS and PAM (ISSC 2003, 2004), are now available that can account for large deformation, contact, non-linearity in material properties and rupture. Some recent supporting literature on numerical simulations of collision and grounding include Kuroiwa (1996), Kitamura et al. (1998, 2001), Endo (2001) and Tornqvist (2003).

Since structures behave in many complex patterns, many special modeling techniques are needed. Challenges involved in analyzing such a high non-linear problem include structural contact, criteria for

material's rupture, crack propagation, among others (Wang et al. 2003).

To analyze a collision or grounding accident involving high non-linearity, contact, friction and rupture, the explicit methodology is suitable. The required calculation efforts are fewer than the commonly used implicit methods. Convergence of calculations is much easier to realize.

3. BENCHMARKING PARTICULARS

This section describes the scaled test models used to compare with the numerical model as well as the finite element tools and general parameters used in the numerical analysis.

3.1 *Mechanical Test*

The prototype laboratory tests reported by Wang et al. (2000) were selected for benchmarking the numerical simulation approach. This series of mechanical tests was designed to cover various collision and grounding scenarios. The tests also provided valuable data related to the major failure mechanisms. Because of these attributes, it made an excellent test bed for investigating and comparing numerical simulations of this complex structural interaction.

Of the nine tests, three (tests P-50, P-200 and C-200) were selected for numerical modeling and comparison in this study. Test P-50 stands for the case of 50 mm radius (sharp) indenter cone positioned on plate; P-200 is the case of 200 mm radius (blunt) indenter cone positioned on plate; and C-200 stands for the case of 200 mm radius (blunt) indenter cone directly on the intersection of main supporting web members. These test cases were selected since they allow comparisons between indenter profiles (sharp vs. blunt) as well as between contact on plate only (i.e., between the support structure) versus contact at an intersection of the support structure. These differences in the test cases result in different failure modes being observed as well as resistance characteristics representative of ship-to-ship collisions. Table 1 provides a summary of the different scaled test parameters used this exercise.

Table 1. Selected Benchmark Testing

Feature	P-50	P-200	C-200
Scaled Tests			
Indenter	50mm, sharp	200mm, blunt	200mm, blunt
Impact location	Shell plate (between supports)	Shell plate (between supports)	Intersection of support member
Initial failure mechanisms	Rupture in shell plate	Rupture away from contact zone	Buckling of support member
Numerical Model			
Mesh	Shell element	Shell element	Shell element
No. elements	18,000	15,000	17,000
CPU time	60 hours	20 hours	25 hours

Figure 1 shows a schematic of the test bed (upper image), and a picture of the actual test setup (lower image). The double hull section was bolted on to strong support frames. The indenters, which are polished rigid cones, were pushed downward, penetrating the double hull section. The rigid cones were pushed very slowly so that dynamic effects were considered to be negligible. Additional details on the scaled tests can be found in the appendix.

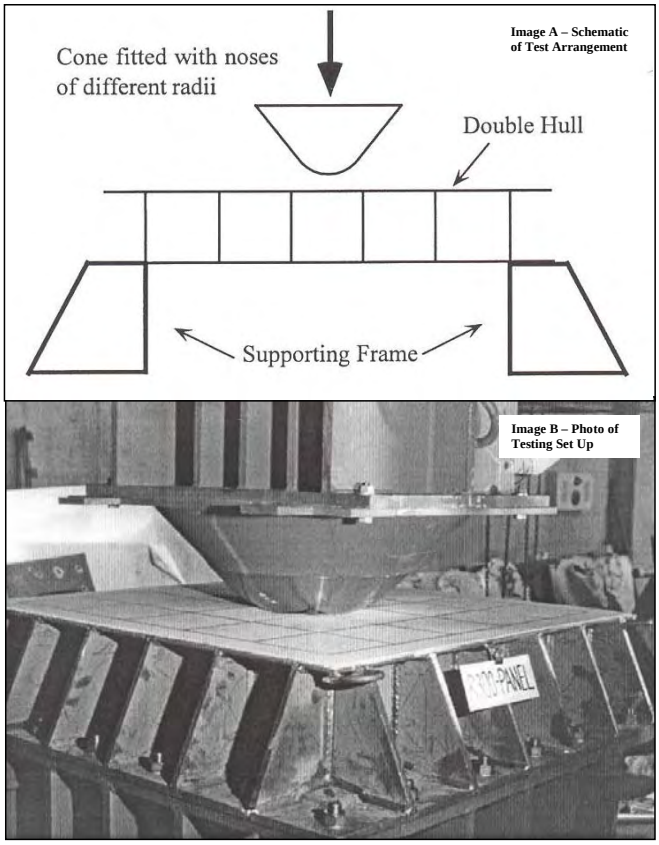

Figure 1. Test Setup Arrangement

3.2 *Numerical Model*

The general purpose finite element program LS-DYNA was used to recreate the tests through numerical simulation. Data pre- and post-processing was done by ANSYS. The explicit analysis solver used by LS-DYNA provided a powerful tool for a fast solution of this nonlinear collision problem.

The double hull test specimens were explicitly modeled as thin shell elements. Spacing between the web supporting members and the depth of the double hull were generally divided into eight elements. Coarser and finer element sizes were also tested in the simulation. Selection of element size is a tradeoff between accuracy and speed of calculations.

The indenter cones were modeled as rigid body. Figure 2 shows the meshed model used to represent the P-200 test case listed in Table 1.

The indenter cones were slowly pushed into the double hull test bed to reflect the quasi-static testing condition. Attention in calculation was paid to the selection of velocity of the indenter to achieve a reasonable balance between calculation accuracy and cost (CPU time).

The dynamic energy was monitored and ensured that it was small and the majority of impact energy was dissipated in the deformed structures. In addition, structural damping was added to further damp out any possible dynamic vibration energy. Hence, the simulated progress was close to quasi-static results from the laboratory tests.

Vertical support boundary conditions were provided along the supporting frame locations. Bolted connection points were modeled as fixed points. The surface slip between the specimen and the test bed, which would likely occur under the large deformation, was not accounted for in the modeling. This aspect will be discussed further in the results and discussion section of this paper.

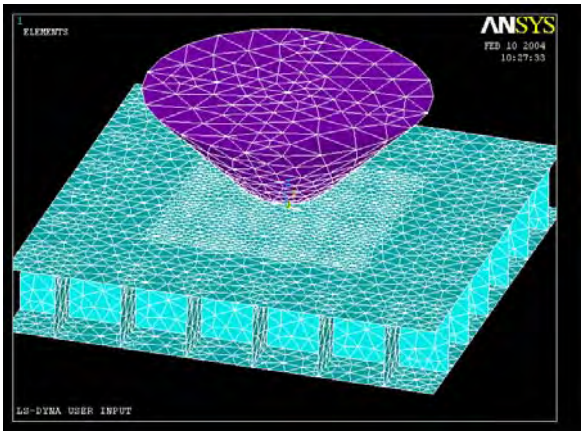

Figure 2. 3-D Image of FEM Model

Since only limited mechanical properties were available on the test set up, typical mild steel material properties were assumed based on Salmon and Johnson (1996). These properties are shown in Table 2. The stress and strain in the table are engineering stress and strain which need to be converted into true values for the simulation.

Table 2. Material properties of steel used in simulation

Yield Strength (N/mm^2)	Ultimate Strength (N/mm^2)	Rupture Strain	Young's Modulus (N/mm^2)	Poisson Ratio
282	400	0.35	200000	0.3

The material was modeled as kinematic hardening material with strain rate dependency. The strain rate effect is accounted for using the Cowper-Symonds model which scales the yield stress by the strain rate dependent factors, though this effect is not critical in a quasi-static test.

Material failure was considered in the model using strain failure criterion. If the calculated effective plastic strain for any element exceeds the predefined value, the element will be removed from the model and the simulation continues with the eroded model.

Under normal dry surface conditions, the friction coefficient on mild-steel-on-mild-steel surface is 0.74 for static friction and 0.57 for sliding friction. However, since the indenter had a polished surface, these values were reduced by about 25%. Therefore, the friction coefficient used in the simulation was 0.55 for static friction and 0.43 for sliding friction.

4. RESULTS COMPARISON

Three main parameters were used to compare the simulation to the test results. These parameters included:

1. Energy Absorption – This is one of the most commonly used parameters used in verification of these types of structural interactions problems. Specifically, it is the energy being absorbed as the indenter is pressed into the double hull test bed.
2. Applied Load – This is often used in more accurate and advanced calculation approaches, and provides a better indication of different failure events and the resulting load and deformation changes throughout the entire loading process.
3. Progressive Damage – This is the overall observed behavior of the structural interaction (i.e., rupture, buckling, large deformations, etc.).

To allow comparison between the test and numerical simulation results, the first two parameters, load and energy, are plotted with indenter displacement. To compare the progressive damage behavior, images of the double hull structure from the test and numerical simulation are presented.

4.1 *P-50 Test Results*

The P-50 test represents a case with a relatively sharp faced indenter driven between support members (i.e., on the plate). The load-indentation curves and absorbed energy-indentation curves are presented in Figure 3. For this case, initial failure is in the form of rupture of the outer shell due to sharp indenter. Once occurred, ruptures begin to tear toward the adjacent support structure. As the indenter is driven further into the structure the load begins to increase again as the indenter comes in contact with the adjacent support structure. Some initial buckling of the support members occurs resulting in some reduced load, but the indenter is now in contact with a large surface and the friction forces gradually increase as the plate and support structure is forced down and outward. The load continues to increase until the support member intersections eventually buckle and there is a notable reduction in load. Note that the indenter is driven to a depth 0.2 meter, which is depth of the double hull structure.

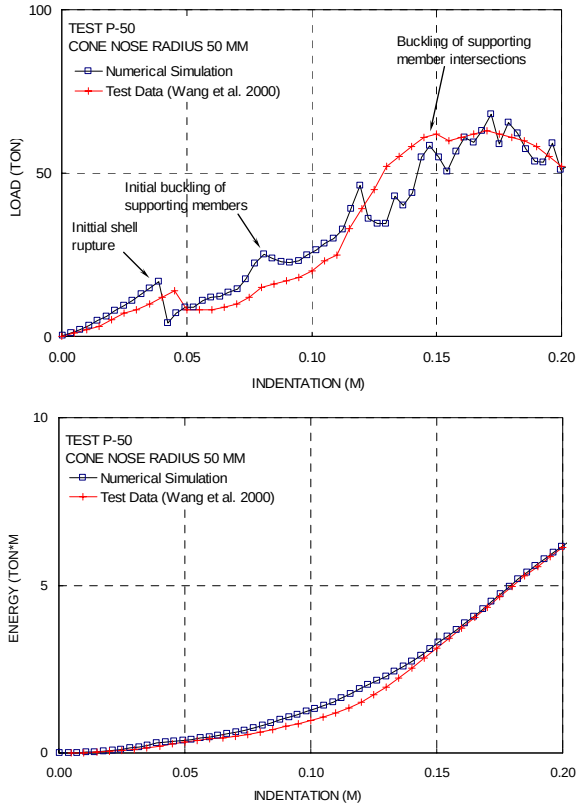

Figure 3. Load and Absorbed Energy Curves, test P-50

When reviewing the plots, the numerical simulation results compare well both with regards to load and energy absorption as the indenter is pushed further into the double hull structure. The results are a good indication the rupture and buckling modeling parameters used in the numerical model are representative of the actual behavior observed in the test. Additionally, it is important to note that the load indentation curves for the simulation are relatively smooth with moderate jumps at particular failure points indicating both the time steps and the mesh size are adequate for the simulation.

Further comparison between the numerical and test results is in the form of the observed damage behavior. Figure 4 shows an image of

the simulation (top) and a picture of the damage in the test specimen. In this case it is noted that although the load and energy results matched, the rupture behavior of the outer shell, the rupture lines did not tear in the same direction. Specifically, the simulation predicted tearing of the plate toward the support member intersections and the test results tore toward the center of the support members. For this case, the rupture behavior of the outer plate was found to be driven by the element size and orientation at the initial contact point of the indenter. This is discussed in more detail in Section 5.3.

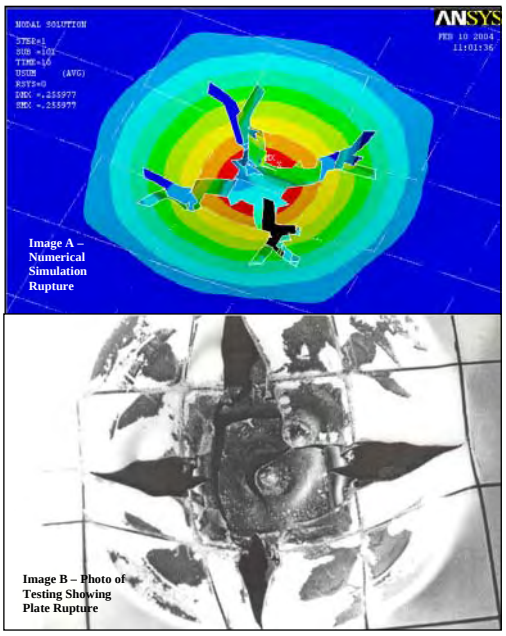

Figure 4. Progressive Damage Comparison, Test P-50

4.2 *P-200 Test Results*

The P-200 test represents a case in which a relatively blunt faced indenter is driven between support members (i.e., on the plate). The load-indentation curves and absorbed energy-indentation curves are presented in Figure 5. For this case, initial failure is in the form of buckling of the adjacent support members due to the large contact region of the indenter. Although buckling occurs, the load continues to increase due to the large contact area and load transfer within the double hull structure.

When reviewing the plots, the numerical simulation results compare well both with regards to load and energy absorption for the initial indentation (i.e., up to 0.12 m). However, there is a notable deviation in load as the indenter exceeds 0.12 m, with the numerical simulation predicting higher overall load and energy absorption than the test results.

Further investigation into this indicated that this is caused by the modeled boundary conditions. The numerical model was found to have more rigid boundary conditions than the bolted connections used in the tests. This was not observed to be an influencing factor for the P-50 test case (See Figure 3). However, unlike the P-50 test case where the sharp indenter tends to rupture the shell plating with only localized deformation of the test bed, the P-200 blunt faced indenter comes in contact with the adjacent supports which tends to cause a more global response (i.e., spreading deformation beyond the contact region) in the test bed. Hence the P-200 results are more dependent on the boundary conditions restraining the overall test bed particularly as the indenter passes midway through the double hull structure. This is also observed by the larger loads and energy absorption in the P-200 cases as compared to the P-50 case. This boundary condition problem will be discussed in more detail in Section 5.1.

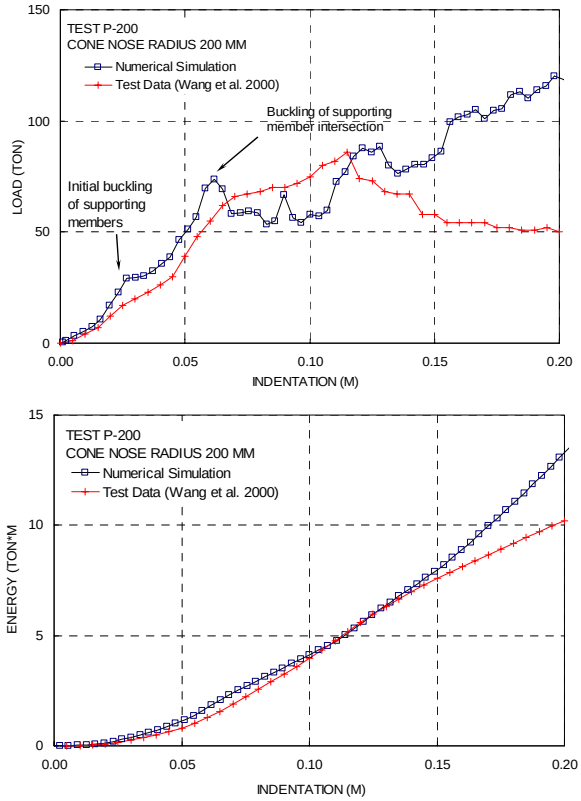

Figure 5. Load and Absorbed Energy Curves, Test P-200

Comparisons between the observed structural behaviors of the double hull were found to be similar. Figure 6 shows an image of the simulation (top) and a picture of the damage in the test specimen.

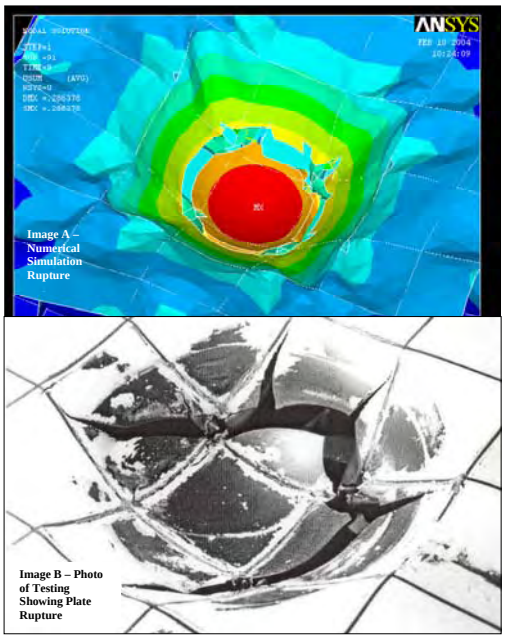

Figure 6. Progressive Damage Comparison, Test P-200

Unlike the P-50 case, the outer shell region at the center of the indenter is deformed and no rupture occurs. Instead rupture occurs along the outer regions outside of the adjacent support structure. In this case, the location of rupture and the general buckling and crushing behavior observed in the numerical model are very similar to the behavior observed in the test.

4.3 *C-200 Test Results*

The C-200 test represents a case in which a relatively blunt faced indenter is driven on top of an intersection of two support members (i.e., cruciform). The load-indentation curves and absorbed energy-indentation curves are presented in Figure 7. For this case, initial failure is in the form of local buckling of the support members beneath the indenter. Although buckling occurs, the load continues to increase due to the large contact area and load transfer within the double hull structure. Eventually, as the indenter is driven over 0.13m. At this point buckling of adjacent support intersections occurs, and there is a noted spread of the outer shell rupture and reduction in load.

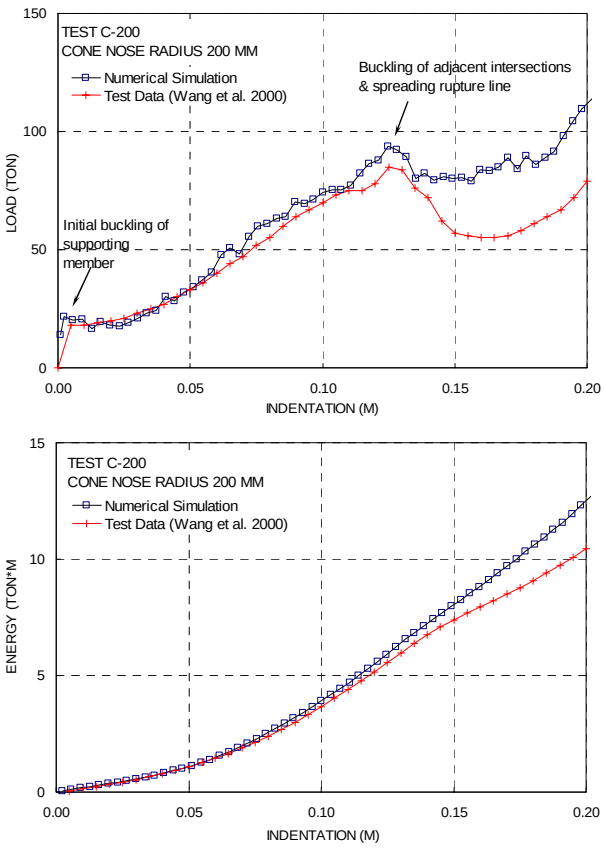

Figure 7. Load and Absorbed Energy Curves, Test C-200

After this point, there is a noted deviation between the test and the numerical results. The numerical simulation tends to predict higher load and energy absorption. This is similar to the behavior observed in the P-200 case and attributed to the modeling boundary conditions. This is discussed in more detail in Section 5.1.

Comparisons between the observed structural behaviors of the double hull were found to be similar. Figure 8 shows an image of the simulation (top) and a picture of the damage in the test specimen.

The outer shell region at the center of the indenter is deformed and no rupture occurs. Rupture occurs along the outer regions just inside of adjacent support structure. In this case, the location of rupture and the general buckling and crushing behavior observed in the numerical model are very similar to the behavior observed in the test.

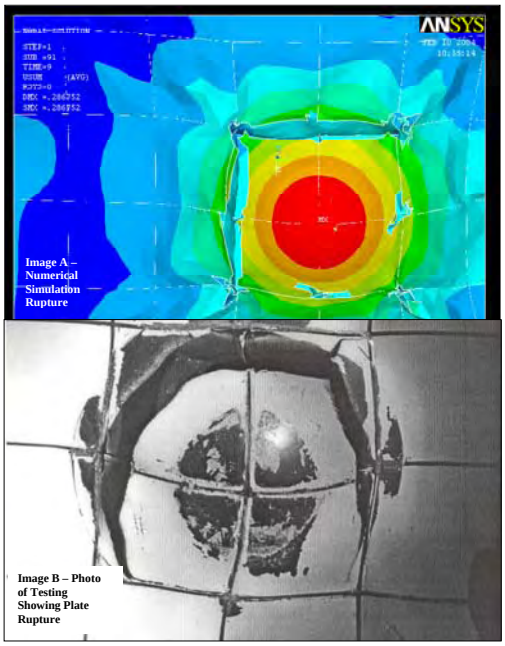

Figure 8. Progressive Damage Comparison, Test C-200

4.4 *Summary*

The comparison indicates the numerical simulation provides very similar results and is capable of capturing the distinctly different failure mechanisms: buckling and rupture. Noted deviations from the test results were investigated further to ensure adequate understanding on what the influencing factors are.

5. DISCUSSIONS

As noted in the results section, some deviations between the numerical simulations and the laboratory test results were observed. Some of the key FEM parameters found to influence the results, specifically in the regions where behavior and load/energy results varied, are discussed in this section.

5.1 *Boundary Conditions*

Simulations deviate somewhat from test results for relatively large indentation. One example is the load-indentation curve of the P-200 test. After about 0.12 m indentation, loads dropped gradually in the test but continued building up in the numerical simulation. This is mainly because beyond this point, the boundary conditions assumed in the simulation have increasing influence on the analysis results.

Color-coded deformation contours as shown in Figure 6 clearly indicates the occurrence of large area deformation beyond the indenter cone contact area and thus the implied high membrane stresses near the support boundary and the bolt connection points in the simulated P-200 model.

In the FEM model, the bolt connections were modeled as fixed points at corresponding locations similar to the actual test set up. The gaps between bolts and holes and the possible slip between two bolted surfaces were not explicitly modeled due to the complexity of the connection. This difference does not have much effect in the initial loading stage when small to moderate hull membrane stress starts to build up. However, close to the final loading stage, as the second hull plate is extensively stretched, very large hull membrane stresses occur. This in turn may overcome the friction resistance between double hull structure and supporting frame, resulting in gap closing and bolt stretching. These factors in the laboratory test will tend to reduce the boundary rigidity and result in an unloading trend. Since this physical situation was not explicitly modeled in the

numerical simulation, some deviations from the test results are anticipated. These influences were confirmed by conducting analysis runs with progressively less rigid model boundary conditions.

5.2 *Mesh Size*

When compared to typical FEM analysis for design purposes, non-linear simulations of a collision event use very fine mesh. To properly capture the local large deformation around a plastic hinge, a non-linear FEM simulation of collision may place 16 elements in one stiffener spacing. Using about 4 elements in one stiffener spacing is generally sufficient for a buckling or ultimate strength analysis. A conventional elastic FEM analysis for design verifications often uses 1 element for the same stiffener spacing. Alternatively, analytical formulae derived for evaluating structural damage characteristics (e.g., failure patterns) such as those summarized by Wierbicki (1992-1999) and Wang (2002) may be used to determine relevant mesh size.

In this study, different element sizes were tested for both accuracy and efficiency. When four elements were used for the depth of the double hull, the predicted load-indentation curve became unstable and fluctuating. The general buckling failure mode is still captured, but the damage progress is not very smooth. Eventually in the depth direction, 8 (triangular) elements were chosen because of the good predictions of load-indentation curves and the reasonable cost (CPU time) as listed in Table.1. More refined elements can also be used but this comes at the expense of increased CPU time.

5.3 *Element Shape and Orientation*

Element shape has some effects on the FEM results depending on the general mesh feature of the model. For shell type elements, quadrilateral elements are generally preferred over triangular elements because the former usually generates fewer elements with the same mesh size.

In this study, both quadrilateral and triangular elements were used in different test cases for comparison purposes. It was found that for the same mesh size, quadrilateral element model tends to rupture and buckle along the predefined node lines since these lines are in regular patterns and well defined as the plastic hinge lines. Conversely, triangular element models had a more irregular mesh pattern that is difficult to lead cracks to some specific direction. The general rupture and buckling behavior of the triangular element model tends to match the experiment test results better than the quadrilateral element model. It is important to note that this observation is only valid for the mesh size we used in the simulation. The difference between element shapes will tend to be reduced if a very fine mesh is applied, but again this comes at the expense of CPU time.

Element orientation also plays a role in determining where the tearing lines go once initiated. For example in Figure 4 of the sharp indenter case P-50, the simulated tearing lines do not fully follow those observed in the test. In the simulation, tearing lines have a tendency to run towards specific directions as a result of localized high stress caused by a combined effect of relatively coarser element sizes and element orientation. This can lead to distortion in tearing lines, especially for the sharp indenter P-50 case for which the element mesh size is relatively large comparing to the indenter cone size. Additional simulations were run and confirmed that a finer mesh with properly selected element orientation tended to result in tearing directions similar to those observed in the laboratory tests.

5.4 *Rupture Strain Used in Analysis*

A major challenge in nonlinear finite element analysis is the prediction and simulation of initiation and propagation of fracture (ISSC 2003). This is essential for members subject to extensive membrane stretching, while it is usually less important for axial crushing.

The most commonly used assumption is that fracture occurs when the ‘‘equivalent strain’’ reaches a critical value. Efforts have been devoted to calibration of this critical value from large-scale tests, real-life observations or tensile tests (i.e., Kitamura 1996, Wang et al. 2002). Element size has been viewed as perhaps the most critical parameters for determining critical rupture strain, and there are some studies addressing this topic (Simonsen et al. 2000, ISSC 2003).

It is noted that this assumption is convenient for both nonlinear finite element analysis and analytical solutions. However, it is not fully justified theoretically. More refined models that consider material behavior around the crack tip are being developed (Simonsen and Tornqvist 2004). It is expected that more rational rupture criteria will emerge that more properly reflect the material behavior and also are easy to be incorporated into a numerical simulation scheme.

The rupture strain used in this study has been listed in Table 2 with other material properties. Over the course of the exercise, different rupture strains were run to investigate sensitivities. Obviously, lower rupture strain results in lower resistance and lower energy absorption capacity. The percentage reduction, however, depends on the general failure mode and damage sequence involving the steel rupture and/or buckling. The rupture strain mainly controls the steel rupture failure. For the tested cases in this exercise, we found that a 30% reduction of rupture strain generally causes 20-25% reduction of energy absorption capacity near the final loading stage. The load-indentation history curve generally resulted in more spikes and sharp drops after the occurrence of first rupture.

5.5 *Friction*

As part of the exercise, different friction coefficients were evaluated. It was concluded that friction coefficients have only some, but not a significant, influence on the general results of this benchmarking exercise. However, for real ship collision and grounding simulation, the friction effect may become quite significant in case of a long duration and large area contacts.

6. CONCLUSION

The recent industry needs for advanced numerical analysis tools have been driving application of nonlinear FEM for analysis of ship collisions.

This paper presented a study that aims to verify and benchmark numerical simulation approach. Due to the complex nature of the collision problem, a significant effort was made to ensure adequate understanding and proper selection of the many variables involved in this finite element analysis.

Comparisons were made between FEM numerical results and laboratory test results of a scaled double hull structure representing ship-to-ship collision/grounding scenarios. The general structural responses (i.e., load and energy results) and major failure modes determined from the FEM compared well with the laboratory tests. Some specific FEM parameters were discussed, including boundary conditions, mesh size, element shape and orientation, rupture strain and friction. The focus is to match FEM simulation to the best possible with test observations.

This exercise confirms the validation of the numerical simulation technique in application on the ship collision problems and provides insight and guidance into some of the key numerical modeling procedures and controls required in the simulation of these complex structural interaction problems.

ACKNOWLEDGEMENTS

This paper reflects work experiences the first two authors have had while working for ABS Consulting. The authors would like to express their gratitude to ABS Consulting and American Bureau of Shipping for supporting them in the development of this paper.

REFERENCES

Brown, A. and Chen, D., 2001. Probabilistic Method for Predicting Ship Collision Damage, Oceanic Engineering International.

Endo, H., and Yamada, Y., 2001. The Performance of Buffer Bow Structures against Collision (1st Report: Collapse Strength of the Simplified Structure Models). Journal of the Society of Naval Architects of Japan, Vol. 189, 209-217.

ISSC, 2003. Committee V.3 Collision and Grounding. 15th International Ship and Offshore Structures Congress (ISSC), San Diego, August 11-15.

ISSC, 2004. ISSC V.1 home page, www.issc-collisiongrounding.org, ISSC Committee V.1 Collision and Grounding, International Ship and Offshore Structures Congress.

Kitamura O., 2001. FEM approach to the simulation of collision and grounding damage. The second International Conference on Collision and Grounding of ships. Copenhagen, Denmark, July 1-3.

Kitamura, O., Kuroiwa, T., Kawamoto, Y. and Kaneko, E., 1998. A Study on the Improved Tanker Structure against Collision and Grounding Damage. Proceedings of the 7th PRADS, 173-179.

Kuroiwa T. 1996. Numerical simulation of actual collision and grounding experiments. International Conference on Design and Methodologies for Collision and Grounding Protection of Ships, San Francisco.

Paik J.K., Chung J.Y., Choe I.H., Thayamballi A.K., Pedersen P.T., Wang G., 1999. On rational design of double hull tanker structures against collision. SNAME annual meeting, Baltimore MD.

Pedersen, P.T., 2002. Collision risk for offshore structure, Journal of Engineering for the Maritime Environment, Proceedings of the Institution of Mechanical Engineers, 216:M1, 29-44.

Salmon, C.G., Johnson, J.E., 1996. Steel Structures, Design and Behavior. Fourth Edition, Harper Collins.

Simonsen, BC., 1997 Ship grounding on rock: I & II., Marine Structures, 10:519–84.

Simonsen, B.C., Lauridsen, L.P., 2000. Energy absorption and ductile fracture in metal sheets under lateral indentation by a sphere, International Journal of Impact Engineering, 24, 1017-1039.

Simonsen, B.C., Tornqvist, R., 2004. Experimental and numerical modeling of ductile crack propagation in large-scale shell element, Marine Structures, 17, 1-27.

Suzuki, K., Ohtsubo, H., Sajit, C., 2000. Evaluation method of absorbed energy in collision of ships with anti-collision structure. Ship Structure Symposium on "Ship Structures for the New Millennium: Supporting Quality in Shipbuilding, Arlington, VA, 13-14 June.

Tornqvist, R., 2003. Design of crashworthiness ship structures, Technical University of Denmark, Ph.D. thesis.

Wang, G., Atita, K., Liu, D., 2000. Behavior of a Double Hull in a Variety of Stranding or Collision Scenarios. Marine Structures, Vol. 13 (2000), pp.147-187.

Wang G., Spencer J., Chen, Y.J., 2002. Assessment of ship's performance in accidents. Marine Structures, 15, 313-333.

Wang G., 2002. Some recent studies on plastic behavior of plates subjected to very large load. Journal of Ocean Mechanics and Arctic Engineering, ASME, 124, 3, 125-131.

Wang G., Jiang DJ, Shin Y., 2003. Consideration of collision and contact damage risks in FPSO structural designs. OTC-15316. Offshore Technology Conference (OTC'03), 5-8 May 2003, Houston, TX.

Wierzbicki, T., 1992-1999. Reports, joint MIT-industry program on tanker safety.

APPENDIX

The test series of Wang et al. (2000) includes nine quasi-static tests to investigate the behavior of a scaled double hull structure. These tests were designed to combine the pressing indenter cones of different nose radii with three major contact locations representing different collision scenarios.

Figure 1 shows a schematic of the test bed (upper image), and a picture of the actual test setup. The overall dimensions are shown in Figure A.1.

The double hull section was bolted on to strong support frames. The test pieces were constructed of 2.3 mm thick mild steel (yield point = 282 N/mm^2). This includes both the two plates representing the inner and outer shell plating of a ship and the main support structures, which represent the web transverses and horizontal stringers. The depth of the double hull was 200 mm. The main support structure is constructed in a grid, evenly spaced at 200 mm in the transverse and longitudinal directions.

The indenters were pushed slowly downward and penetrated the double hull section. Five different indenters with spherical nose radii of 300, 200, 100, 50, and 10 mm were used to simulate various striking vessels.

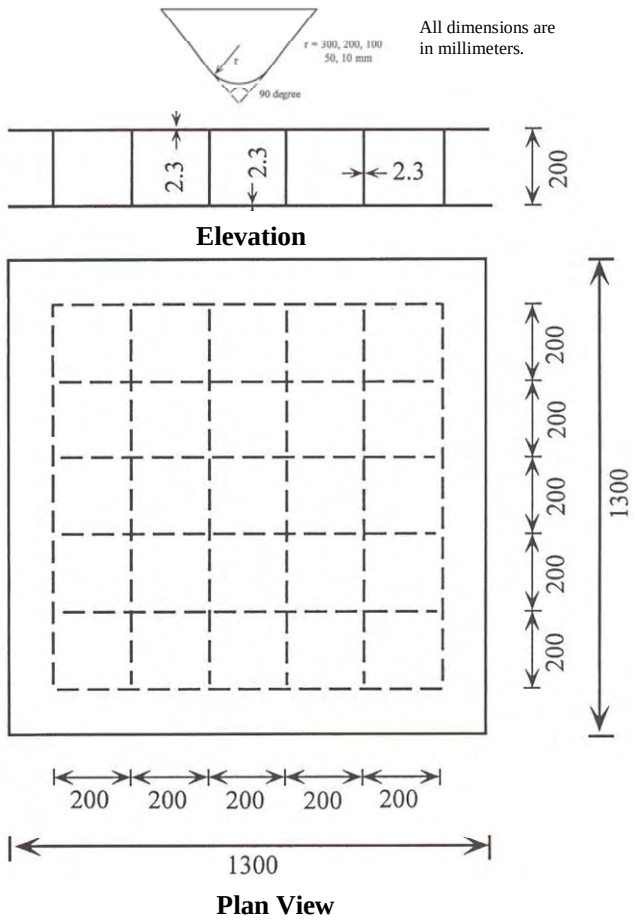

Figure A.1. Details of tested double hull

APPENDIX B

FSRU MODEL

APPENDIX C
TANKER COLLISION

External Energy Calculation

Run Ref: ***Example Kinetic Energy Calculation for Tanker / FSRU Collision***

This worksheet calculates the external energy loss from the collision of two ships. The equations are from *On Impact Mechanics in Ship Collisions,* by P. Pedersen and S. Zhang, Marine Strucutures, vol. 11 1998.

units $MJ := 1000000J$ $tonnes := 1000kg$

Input Varibles

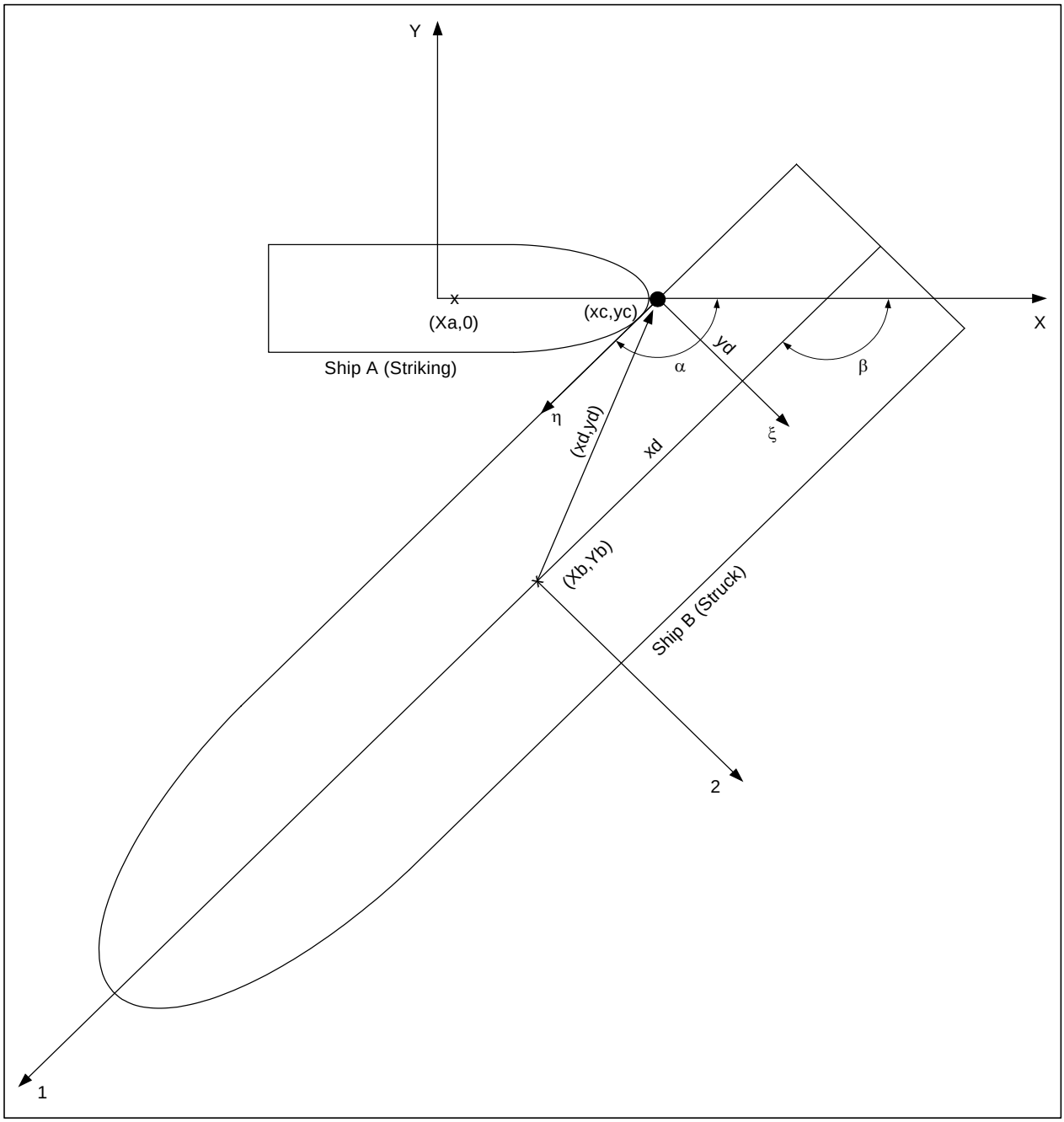

Mases

Mass of Ship A (striking)	$Ma := 245000tonnes$
Mass of Ship B (struck)	$Mb := 190000tonnes$
Added mass of ship A in surge direction	$max := .05$
Added mass of ship A in sway direction	$may := .85$
Added mass of ship B in surge direction	$mb1 := .05$
Added mass of ship B in sway direction	$mb2 := .85$
Rotational added mass of ship A	$ja := .21$
Rotational added mass of ship B	$jb := .21$

Velocities

Velocity of ship A (striking) in surge direction	$Vax := 2.57\frac{m}{s}$
Velocity of ship A in sway direction	$Vay := 0\frac{m}{s}$
Velocity of ship B (struck) in surge direction	$Vb1 := 0\frac{m}{s}$
Velocity of ship B in sway direction	$Vb2 := 0\frac{m}{s}$

Ship Geometery

Length of ship A	$La := 288m$
Length of ship B	$Lb := 263.7m$
Breadth of ship B	$Ba := 65m$
Radius of ship mass inertia	$Ra := \frac{La}{4}$
	$Rb := \frac{Lb}{4}$

Collision Varibles

Distance along the y axis to collision point	$yc := 0m$	
Distance along the x axis to collision point	$xc := \frac{La}{2}$	
Distance along the x axis to center of ship A	$xa := 0m$	
Distance along the x axis to center of ship B	$xd := \frac{Ba}{2}$	$xd := xd + 0.01m$
Distance along the y axis to center of ship B	$yd := 0m$	
Angle between ship A and the x axis	$\alpha := 90deg$	
Angle between ship B and the x axis	$\beta := 90deg$	

Distance between center of ship B and collision point from (xd,yd) direction	$xyd := \sqrt{xd^2 + yd^2}$	
Angle between ship A and (xd,yd) direction	$k := atan\left(\frac{yd}{xd}\right)$	$k = 0$
Distance along the x axis of ship B to collision point	$xb(xc,\beta) := xc + xyd \cdot cos(k - \beta)$	$xb(xc,\beta) = 144\,m$
Distance along the y axis of ship B to collision point	$yb(yc,\beta) := yc + xyd \cdot sin(k - \beta)$	$yb(yc,\beta) = -32.51\,m$

Coefficients

Coefficient of Restitution (0 is fully plastic collision)	$e := 0$
Cofficient of Friction	$\mu o := .6$

Equations

$$Da\zeta(xc,yc,\beta,\alpha) := \frac{1}{1+max}\sin(\alpha)^2 + \frac{1}{1+may}\cdot\cos(\alpha)^2 + \frac{1}{1+ja}\cdot\frac{\left[yc\cdot\sin(\alpha) - (xc-xa)\cdot\cos(\alpha)\right]^2}{Ra^2}$$

$$Da\eta(xc,yc,\beta,\alpha) := \left| \begin{array}{l} a \leftarrow \frac{1}{(1+max)}\cdot\sin(\alpha)\cdot\cos(\alpha) - \frac{1}{1+may}\cdot\sin(\alpha)\cdot\cos(\alpha) \\ b \leftarrow \frac{1}{1+ja}\cdot\frac{\left[yc\cdot\sin(\alpha) - (xc-xa)\cdot\cos(\alpha)\right]\cdot\left[yc\cdot\cos(\alpha) + (xc-xa)\cdot\sin(\alpha)\right]}{Ra^2} \\ a+b \end{array} \right.$$

$$Db\zeta(xc,yc,\beta,\alpha) := \frac{1}{1+mb1}\cdot\sin(\beta-\alpha)^2 + \frac{1}{1+mb2}\cdot\cos(\beta-\alpha)^2 + \frac{1}{1+jb}\cdot\frac{\left[(yc-yb(yc,\beta))\cdot\sin(\alpha) - (xc-xb(xc,\beta))\cdot\cos(\alpha)\right]^2}{Rb^2}$$

$$Db\eta(xc,yc,\beta,\alpha) := \left| \begin{array}{l} a \leftarrow \frac{-1}{1+mb1}\cdot\sin(\beta-\alpha)\cdot\cos(\beta-\alpha) + \frac{1}{1+mb2}\cdot\sin(\beta-\alpha)\cdot\cos(\beta-\alpha) \\ b \leftarrow \frac{1}{1+jb}\cdot\frac{\left[(yc-yb(yc,\beta))\cdot\sin(\alpha) - (xc-xb(xc,\beta))\cdot\cos(\alpha)\right]\cdot\left[(yc-yb(yc,\beta))\cdot\cos(\alpha) + (xc-xb(xc,\beta))\cdot\sin(\alpha)\right]}{Rb^2} \\ a+b \end{array} \right.$$

$$Ka\zeta(xc,yc,\beta,\alpha) := \left| \begin{array}{l} a \leftarrow \frac{1}{(1+max)}\cdot\sin(\alpha)\cdot\cos(\alpha) - \frac{1}{1+may}\cdot\sin(\alpha)\cdot\cos(\alpha) \\ b \leftarrow \frac{1}{1+ja}\cdot\frac{\left[yc\cdot\sin(\alpha) - (xc-xa)\cdot\cos(\alpha)\right]\cdot\left[yc\cdot\cos(\alpha) + (xc-xa)\cdot\sin(\alpha)\right]}{Ra^2} \\ a+b \end{array} \right.$$

$$Ka\eta(xc,yc,\beta,\alpha) := \frac{1}{1+max}\cdot\cos(\alpha)^2 + \frac{1}{1+may}\cdot\sin(\alpha)^2 + \frac{1}{1+ja}\cdot\frac{\left[yc\cdot\cos(\alpha)+(xc-xa)\cdot\sin(\alpha)\right]^2}{Ra^2}$$

$$Kb\zeta(xc,yc,\beta,\alpha) := \left|\begin{array}{l} a \leftarrow \frac{-1}{1+mb1}\cdot\sin(\beta-\alpha)\cdot\cos(\beta-\alpha) + \frac{1}{1+mb2}\cdot\sin(\beta-\alpha)\cdot\cos(\beta-\alpha) \\ b \leftarrow \frac{1}{1+jb}\cdot\frac{\left[(yc-yb(yc,\beta))\cdot\sin(\alpha)-(xc-xb(xc,\beta))\cdot\cos(\alpha)\right]\cdot\left[(yc-yb(yc,\beta))\cdot\cos(\alpha)+(xc-xb(xc,\beta))\cdot\sin(\alpha)\right]}{Rb^2} \\ a+b \end{array}\right.$$

$$Kb\eta(xc,yc,\beta,\alpha) := \frac{1}{1+mb1}\cdot\cos(\beta-\alpha)^2 + \frac{1}{1+mb2}\cdot\sin(\beta-\alpha)^2 + \frac{1}{1+jb}\cdot\frac{\left[(yc-yb(yc,\beta))\cdot\cos(\alpha)+(xc-xb(xc,\beta))\cdot\sin(\alpha)\right]^2}{Rb^2}$$

$$D\zeta(xc,yc,\beta,\alpha) := \frac{Da\zeta(xc,yc,\beta,\alpha)}{Ma} + \frac{Db\zeta(xc,yc,\beta,\alpha)}{Mb}$$

$$K\zeta(xc,yc,\beta,\alpha) := \frac{Ka\zeta(xc,yc,\beta,\alpha)}{Ma} + \frac{Kb\zeta(xc,yc,\beta,\alpha)}{Mb}$$

$$D\eta(xc,yc,\beta,\alpha) := \frac{Da\eta(xc,yc,\beta,\alpha)}{Ma} + \frac{Db\eta(xc,yc,\beta,\alpha)}{Mb}$$

$$K\eta(xc,yc,\beta,\alpha) := \frac{Ka\eta(xc,yc,\beta,\alpha)}{Ma} + \frac{Kb\eta(xc,yc,\beta,\alpha)}{Mb}$$

Velocities in ζ and η direction

$$\zeta dot(\beta,\alpha) := Vax\cdot\sin(\alpha) + Vay\cdot\cos(\alpha) + Vb1\cdot\sin(\beta-\alpha) - Vb2\cdot\cos(\beta-\alpha)$$

$$\eta dot(\beta,\alpha) := Vax\cdot\cos(\alpha) - Vay\cdot\sin(\alpha) - Vb1\cdot\cos(\beta-\alpha) - Vb2\cdot\sin(\beta-\alpha)$$

Ratio of impact impulses, if |μ| > μo then sliding occurs

$$\mu(xc,yc,\beta,\alpha) := \frac{D\zeta(xc,yc,\beta,\alpha)\cdot\eta dot(\beta,\alpha) - K\zeta(xc,yc,\beta,\alpha)\cdot\zeta dot(\beta,\alpha)\cdot(1+e)}{K\eta(xc,yc,\beta,\alpha)\cdot\zeta dot(\beta,\alpha)\cdot(1+e) - D\eta(xc,yc,\beta,\alpha)\cdot\eta dot(\beta,\alpha)}$$

$$\mu o := sign(\mu(xc,yc,\beta,\alpha))\cdot|\mu o|$$

Final velocity in η direction if sliding

$$\eta T(xc,yc,\beta,\alpha) := \eta dot(\beta,\alpha) - \frac{K\zeta(xc,yc,\beta,\alpha)+\mu o\cdot K\eta(xc,yc,\beta,\alpha)}{D\zeta(xc,yc,\beta,\alpha)+\mu o\cdot D\eta(xc,yc,\beta,\alpha)}\cdot\zeta dot(\beta,\alpha)\cdot(1+e)$$

Energy loss from Sticking

$$E\zeta(xc,yc,\beta,\alpha) := \frac{1}{2}\cdot\frac{1}{D\zeta(xc,yc,\beta,\alpha)+\mu(xc,yc,\beta,\alpha)\cdot D\eta(xc,yc,\beta,\alpha)}\cdot\left(1-e^2\right)\cdot\zeta dot(\beta,\alpha)^2$$

$$E\eta(xc,yc,\beta,\alpha) := \frac{1}{2}\cdot\frac{1}{\frac{1}{\mu(xc,yc,\beta,\alpha)}\cdot K\zeta(xc,yc,\beta,\alpha)+K\eta(xc,yc,\beta,\alpha)}\cdot\eta dot(\beta,\alpha)^2$$

Energy Loss from sticking

$$Estick := E\zeta(xc,yc,\beta,\alpha)+E\eta(xc,yc,\beta,\alpha)$$

$$Estick = 423.935\,MJ$$

Energy loss from Sliding

$$E\zeta s(xc,yc,\beta,\alpha) := \frac{1}{2}\cdot\frac{1}{D\zeta(xc,yc,\beta,\alpha)+\mu o\cdot D\eta(xc,yc,\beta,\alpha)}\cdot\zeta dot(\beta,\alpha)^2\cdot\left(1+e^2\right)$$

$$E\eta s(xc,yc,\beta,\alpha) := \frac{1}{2}\cdot\frac{1}{\frac{1}{\mu o}\cdot K\zeta(xc,yc,\beta,\alpha)+K\eta(xc,yc,\beta,\alpha)}\cdot\left(\eta dot(\beta,\alpha)^2-\eta T(xc,yc,\beta,\alpha)^2\right)$$

Energy Loss from sliding

$$Eslide := E\zeta s(xc,yc,\beta,\alpha)+E\eta s(xc,yc,\beta,\alpha)$$

$$Eslide = 18.162\,MJ$$

Energy Loss

If |μ|<μo energy loss is from sticking, otherwise it is from sliding

$$E(xc,yc,\beta,\alpha) := \begin{cases} E\zeta(xc,yc,\beta,\alpha)+E\eta(xc,yc,\beta,\alpha) & \text{if } |\mu(xc,yc,\beta,\alpha)| < |\mu o| \\ E\zeta s(xc,yc,\beta,\alpha)+E\eta s(xc,yc,\beta,\alpha) & \text{otherwise} \end{cases}$$

Energy loss from ship collision

Use this result ==> $E(xc,yc,\beta,\alpha) = 423.935\,MJ$

Initial Total Kinetic Energy

$$Ei := \left[\frac{1}{2}\cdot(1+max)\cdot Ma\cdot\left(Vax^2+Vay^2\right)\right]+\frac{1}{2}\cdot(1+mb1)\cdot Mb\cdot\left(Vb1^2+Vb2^2\right)$$

$$Ei = 849.555\,MJ$$

Released Energy Ratio (compared to initial total energy)

$$Er := \frac{E(xc,yc,\beta,\alpha)}{Ei}$$

$$Er = 0.499$$

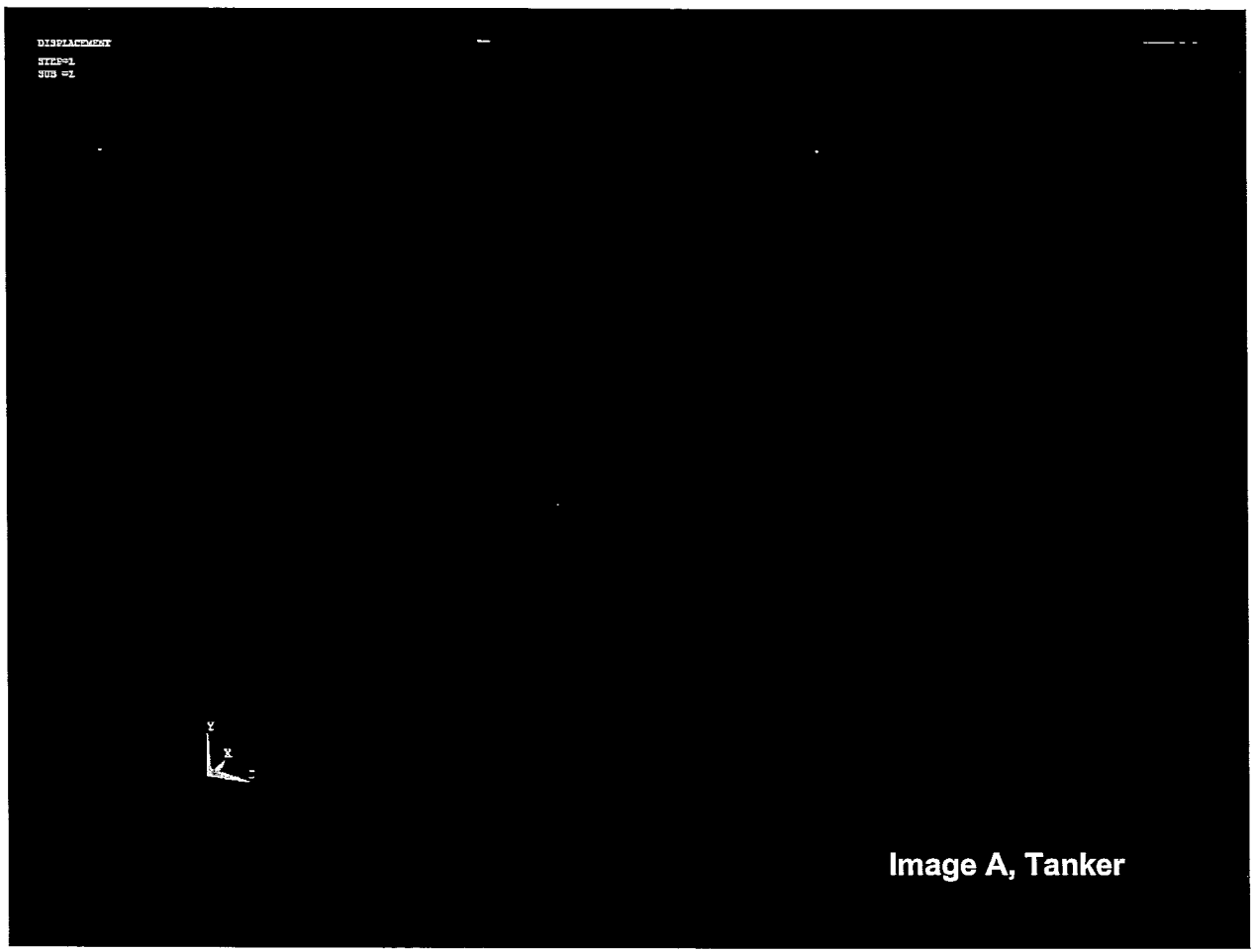

Image A, Tanker

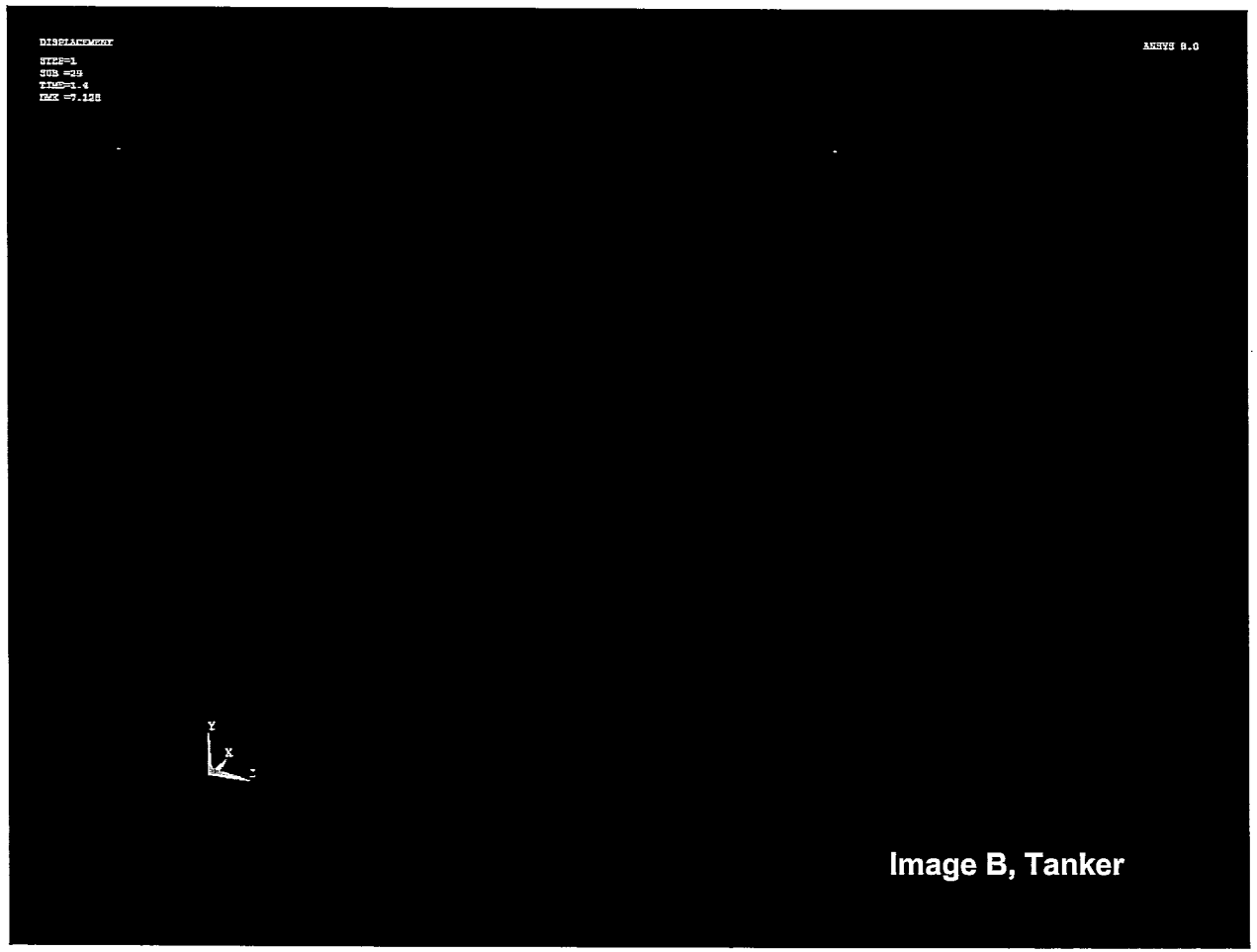

Image B, Tanker

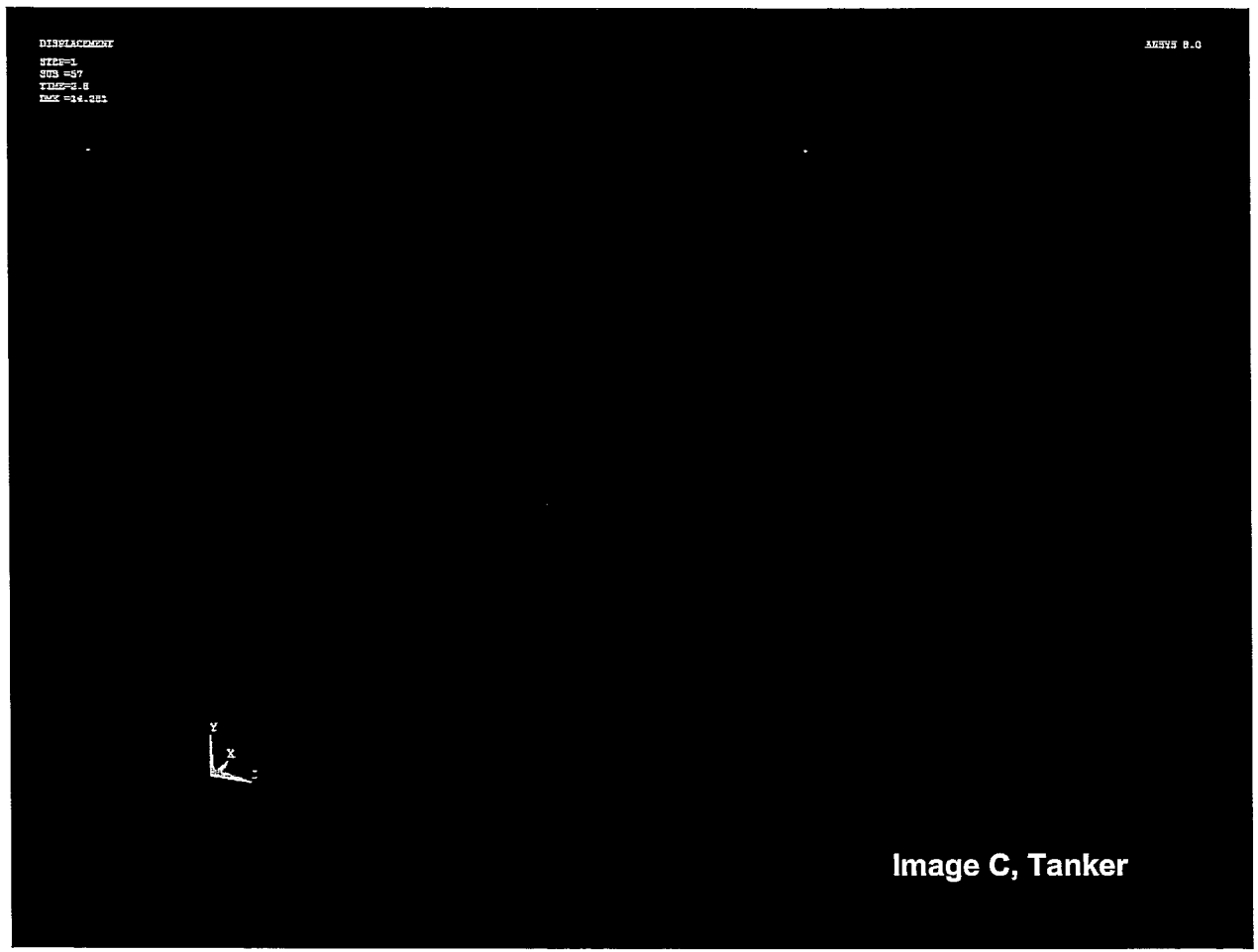

Image C, Tanker

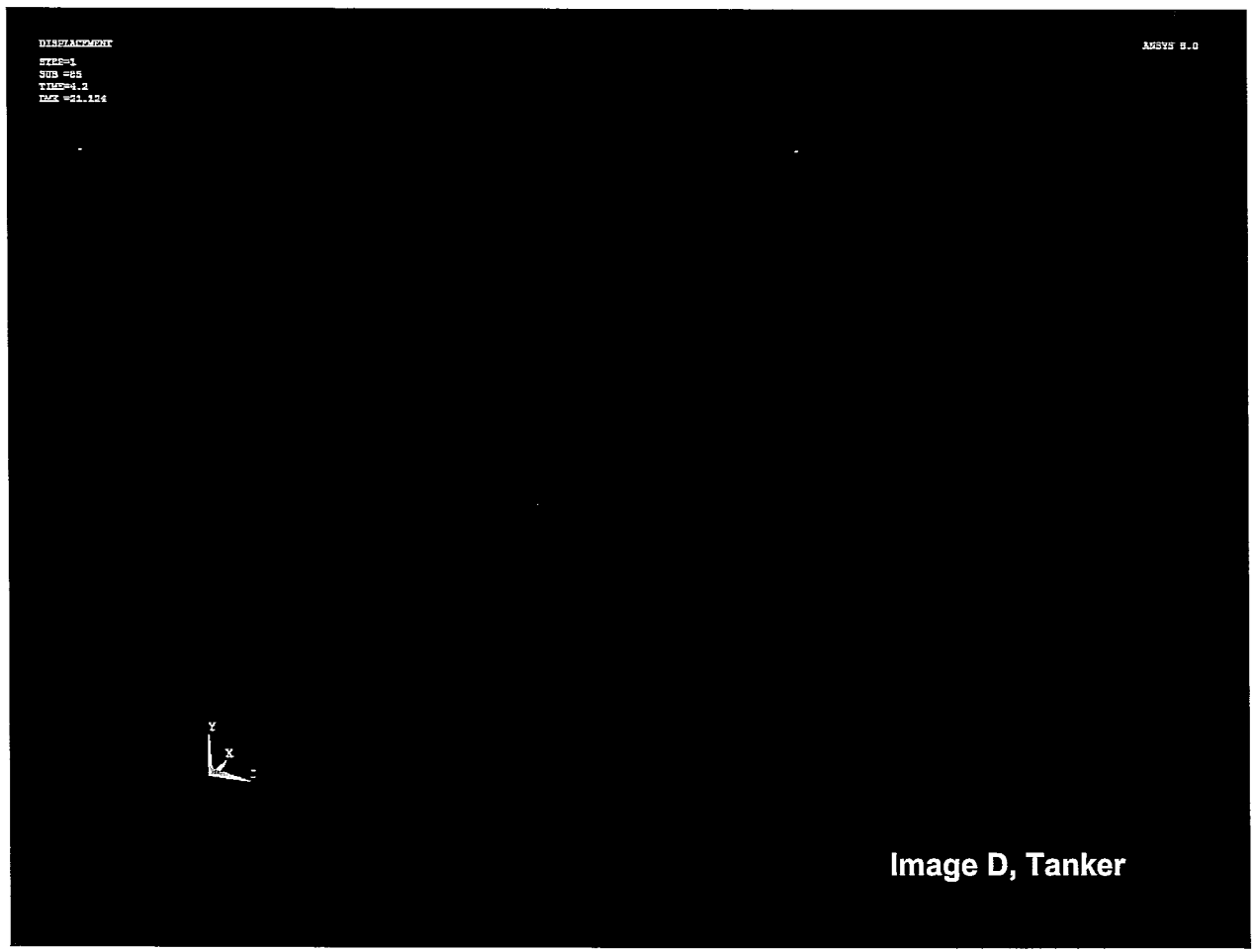

Image D, Tanker

Image A, FSRU (Tanker Case)

Image B, FSRU (Tanker Case)

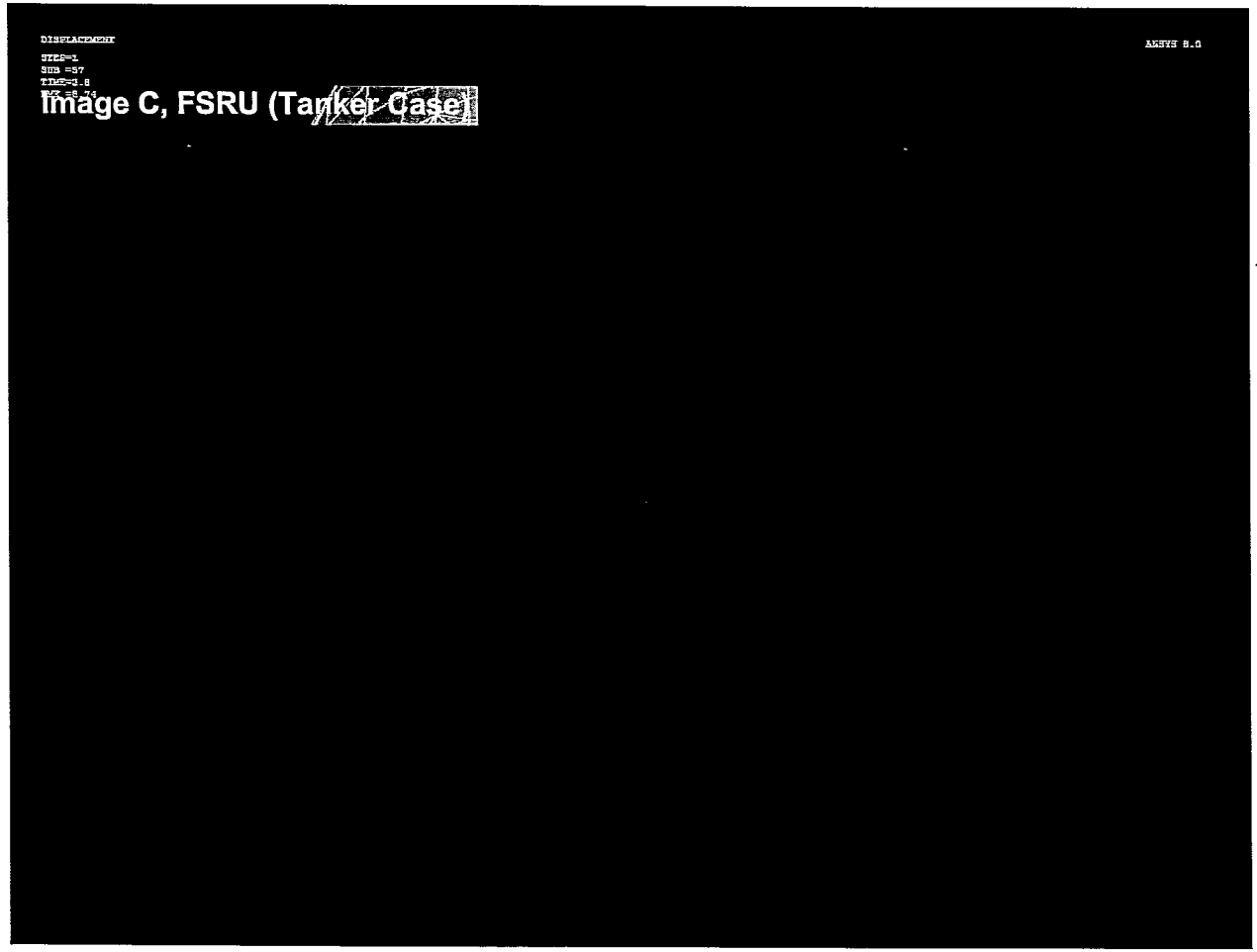

Image C, FSRU (Tanker Case)

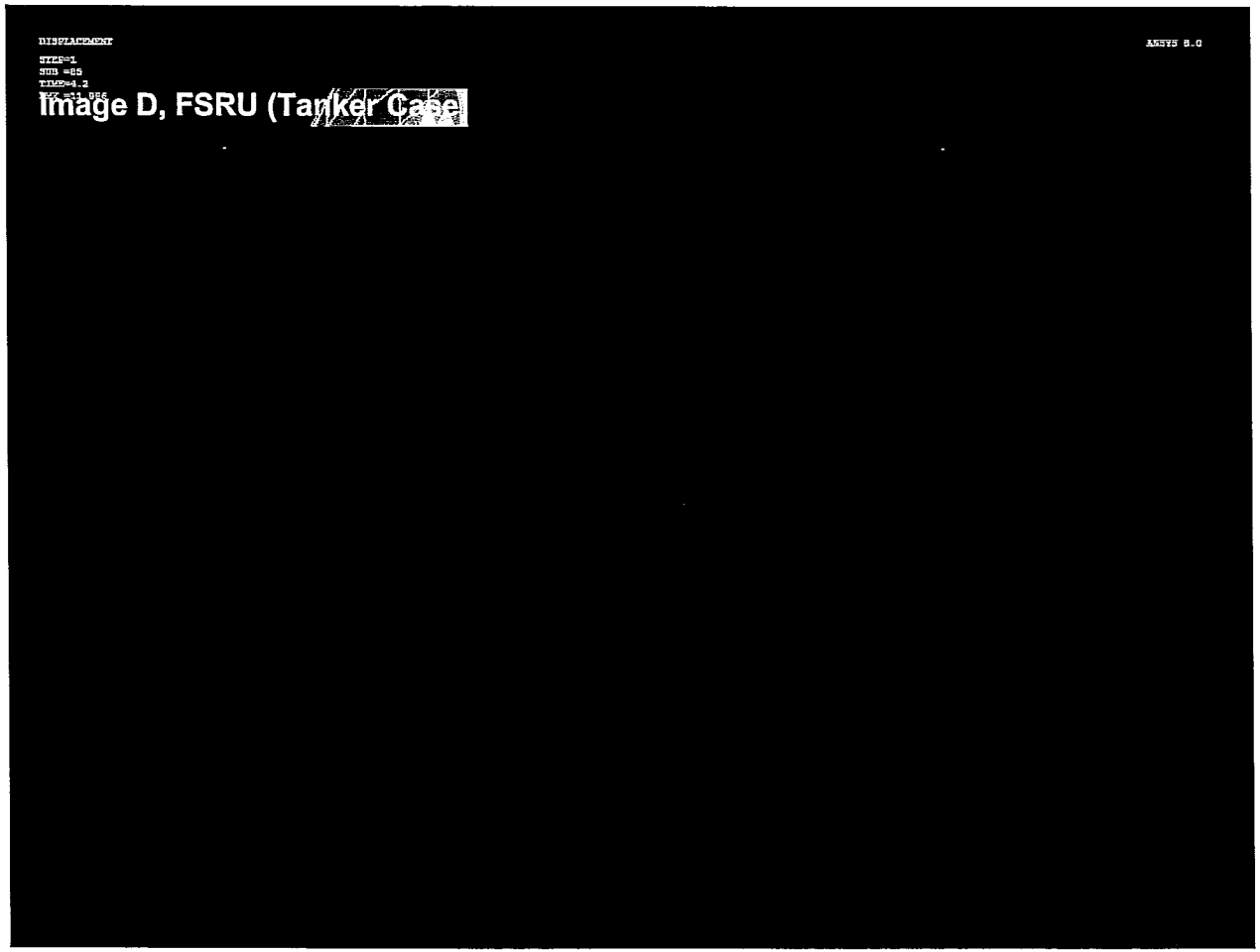

Image D, FSRU (Tanker Case

APPENDIX D

CONTAINER SHIP COLLISION

External Energy Calculation

Run Ref: ***Example Kinetic Energy Calculation for Container Ship / FSRU Collision***

This worksheet calculates the external energy loss from the collision of two ships. The equations are from *On Impact Mechanics in Ship Collisions,* by P. Pedersen and S. Zhang, Marine Strucutures, vol. 11 1998.

units $MJ := 1000000J$ $tonnes := 1000kg$

Input Varibles

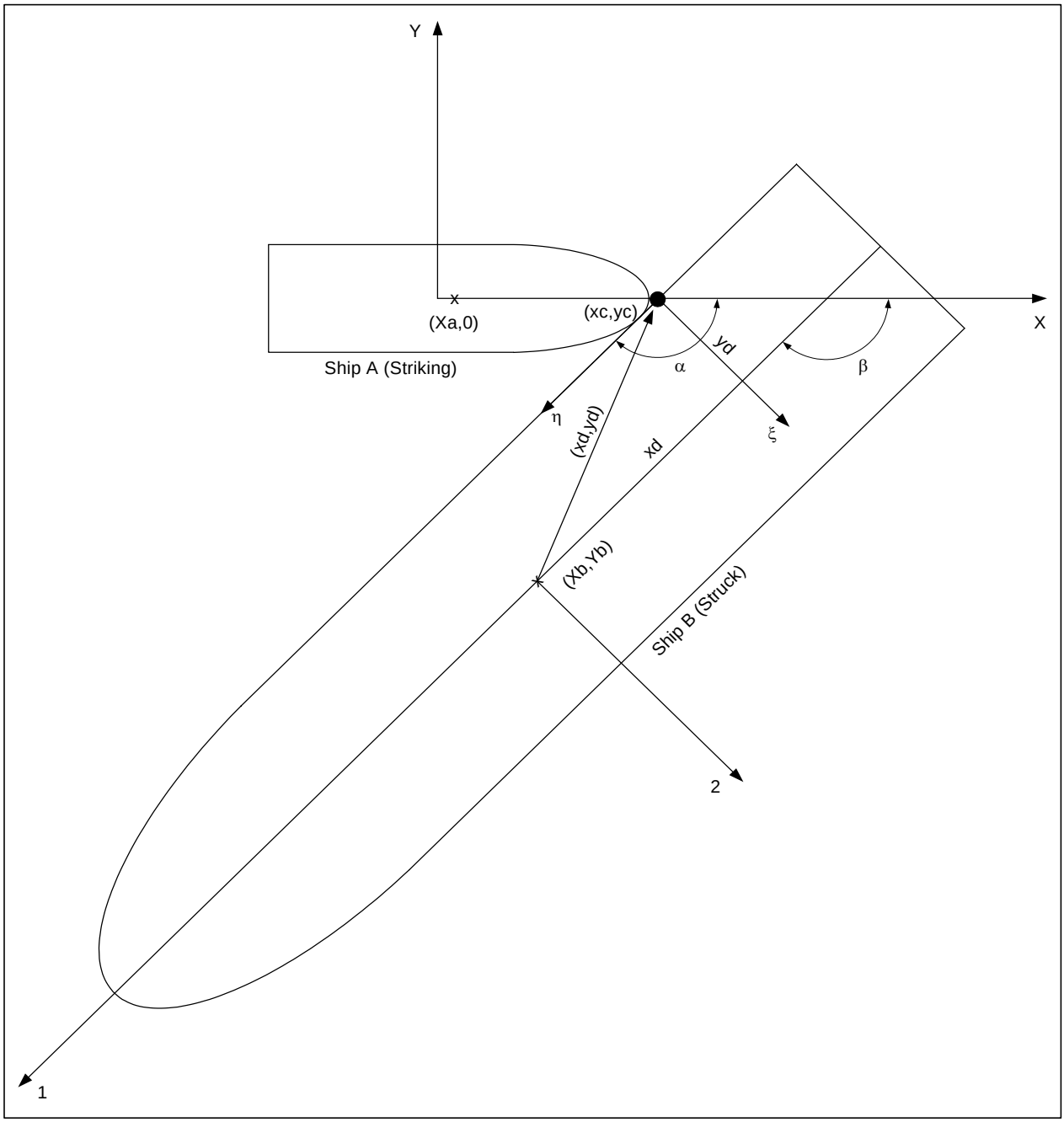

Mases

Mass of Ship A (striking)	$Ma := 88000tonnes$
Mass of Ship B (struck)	$Mb := 190000tonnes$
Added mass of ship A in surge direction	$max := .05$
Added mass of ship A in sway direction	$may := .85$
Added mass of ship B in surge direction	$mb1 := .05$
Added mass of ship B in sway direction	$mb2 := .85$
Rotational added mass of ship A	$ja := .21$
Rotational added mass of ship B	$jb := .21$

Velocities

Velocity of ship A (striking) in surge direction	$Vax := 2.57\frac{m}{s}$
Velocity of ship A in sway direction	$Vay := 0\frac{m}{s}$
Velocity of ship B (struck) in surge direction	$Vb1 := 0\frac{m}{s}$
Velocity of ship B in sway direction	$Vb2 := 0\frac{m}{s}$

Ship Geometery

Length of ship A	$La := 282m$
Length of ship B	$Lb := 263.7m$
Breadth of ship B	$Ba := 65m$
Radius of ship mass inertia	$Ra := \frac{La}{4}$
	$Rb := \frac{Lb}{4}$

Collision Varibles

Distance along the y axis to collision point	$yc := 0m$	
Distance along the x axis to collision point	$xc := \frac{La}{2}$	
Distance along the x axis to center of ship A	$xa := 0m$	
Distance along the x axis to center of ship B	$xd := \frac{Ba}{2}$	$xd := xd + 0.01m$
Distance along the y axis to center of ship B	$yd := 0m$	
Angle between ship A and the x axis	$\alpha := 90deg$	
Angle between ship B and the x axis	$\beta := 90deg$	

Distance between center of ship B and collision point from (xd,yd) direction	$xyd := \sqrt{xd^2 + yd^2}$	
Angle between ship A and (xd,yd) direction	$k := atan\left(\frac{yd}{xd}\right)$	$k = 0$
Distance along the x axis of ship B to collision point	$xb(xc,\beta) := xc + xyd \cdot cos(k - \beta)$	$xb(xc,\beta) = 141\,m$
Distance along the y axis of ship B to collision point	$yb(yc,\beta) := yc + xyd \cdot sin(k - \beta)$	$yb(yc,\beta) = -32.51\,m$

Coefficients

Coefficient of Restitution (0 is fully plastic collision)	$e := 0$
Cofficient of Friction	$\mu o := .6$

Equations

$$Da\zeta(xc,yc,\beta,\alpha) := \frac{1}{1+max}\sin(\alpha)^2 + \frac{1}{1+may}\cdot\cos(\alpha)^2 + \frac{1}{1+ja}\cdot\frac{\left[yc\cdot\sin(\alpha) - (xc-xa)\cdot\cos(\alpha)\right]^2}{Ra^2}$$

$$Da\eta(xc,yc,\beta,\alpha) := \left| \begin{array}{l} a \leftarrow \frac{1}{(1+max)}\cdot\sin(\alpha)\cdot\cos(\alpha) - \frac{1}{1+may}\cdot\sin(\alpha)\cdot\cos(\alpha) \\ b \leftarrow \frac{1}{1+ja}\cdot\frac{\left[yc\cdot\sin(\alpha) - (xc-xa)\cdot\cos(\alpha)\right]\cdot\left[yc\cdot\cos(\alpha) + (xc-xa)\cdot\sin(\alpha)\right]}{Ra^2} \\ a+b \end{array} \right.$$

$$Db\zeta(xc,yc,\beta,\alpha) := \frac{1}{1+mb1}\cdot\sin(\beta-\alpha)^2 + \frac{1}{1+mb2}\cdot\cos(\beta-\alpha)^2 + \frac{1}{1+jb}\cdot\frac{\left[(yc-yb(yc,\beta))\cdot\sin(\alpha) - (xc-xb(xc,\beta))\cdot\cos(\alpha)\right]^2}{Rb^2}$$

$$Db\eta(xc,yc,\beta,\alpha) := \left| \begin{array}{l} a \leftarrow \frac{-1}{1+mb1}\cdot\sin(\beta-\alpha)\cdot\cos(\beta-\alpha) + \frac{1}{1+mb2}\cdot\sin(\beta-\alpha)\cdot\cos(\beta-\alpha) \\ b \leftarrow \frac{1}{1+jb}\cdot\frac{\left[(yc-yb(yc,\beta))\cdot\sin(\alpha) - (xc-xb(xc,\beta))\cdot\cos(\alpha)\right]\cdot\left[(yc-yb(yc,\beta))\cdot\cos(\alpha) + (xc-xb(xc,\beta))\cdot\sin(\alpha)\right]}{Rb^2} \\ a+b \end{array} \right.$$

$$Ka\zeta(xc,yc,\beta,\alpha) := \left| \begin{array}{l} a \leftarrow \frac{1}{(1+max)}\cdot\sin(\alpha)\cdot\cos(\alpha) - \frac{1}{1+may}\cdot\sin(\alpha)\cdot\cos(\alpha) \\ b \leftarrow \frac{1}{1+ja}\cdot\frac{\left[yc\cdot\sin(\alpha) - (xc-xa)\cdot\cos(\alpha)\right]\cdot\left[yc\cdot\cos(\alpha) + (xc-xa)\cdot\sin(\alpha)\right]}{Ra^2} \\ a+b \end{array} \right.$$

$$Ka\eta(xc,yc,\beta,\alpha) := \frac{1}{1+max}\cdot\cos(\alpha)^2 + \frac{1}{1+may}\cdot\sin(\alpha)^2 + \frac{1}{1+ja}\cdot\frac{\left[yc\cdot\cos(\alpha)+(xc-xa)\cdot\sin(\alpha)\right]^2}{Ra^2}$$

$$Kb\zeta(xc,yc,\beta,\alpha) := \left|\begin{array}{l} a \leftarrow \frac{-1}{1+mb1}\cdot\sin(\beta-\alpha)\cdot\cos(\beta-\alpha) + \frac{1}{1+mb2}\cdot\sin(\beta-\alpha)\cdot\cos(\beta-\alpha) \\ b \leftarrow \frac{1}{1+jb}\cdot\frac{\left[(yc-yb(yc,\beta))\cdot\sin(\alpha)-(xc-xb(xc,\beta))\cdot\cos(\alpha)\right]\cdot\left[(yc-yb(yc,\beta))\cdot\cos(\alpha)+(xc-xb(xc,\beta))\cdot\sin(\alpha)\right]}{Rb^2} \\ a+b \end{array}\right.$$

$$Kb\eta(xc,yc,\beta,\alpha) := \frac{1}{1+mb1}\cdot\cos(\beta-\alpha)^2 + \frac{1}{1+mb2}\cdot\sin(\beta-\alpha)^2 + \frac{1}{1+jb}\cdot\frac{\left[(yc-yb(yc,\beta))\cdot\cos(\alpha)+(xc-xb(xc,\beta))\cdot\sin(\alpha)\right]^2}{Rb^2}$$

$$D\zeta(xc,yc,\beta,\alpha) := \frac{Da\zeta(xc,yc,\beta,\alpha)}{Ma} + \frac{Db\zeta(xc,yc,\beta,\alpha)}{Mb}$$

$$K\zeta(xc,yc,\beta,\alpha) := \frac{Ka\zeta(xc,yc,\beta,\alpha)}{Ma} + \frac{Kb\zeta(xc,yc,\beta,\alpha)}{Mb}$$

$$D\eta(xc,yc,\beta,\alpha) := \frac{Da\eta(xc,yc,\beta,\alpha)}{Ma} + \frac{Db\eta(xc,yc,\beta,\alpha)}{Mb}$$

$$K\eta(xc,yc,\beta,\alpha) := \frac{Ka\eta(xc,yc,\beta,\alpha)}{Ma} + \frac{Kb\eta(xc,yc,\beta,\alpha)}{Mb}$$

Velocities in ζ and η direction

$$\zeta dot(\beta,\alpha) := Vax\cdot\sin(\alpha) + Vay\cdot\cos(\alpha) + Vb1\cdot\sin(\beta-\alpha) - Vb2\cdot\cos(\beta-\alpha)$$

$$\eta dot(\beta,\alpha) := Vax\cdot\cos(\alpha) - Vay\cdot\sin(\alpha) - Vb1\cdot\cos(\beta-\alpha) - Vb2\cdot\sin(\beta-\alpha)$$

Ratio of impact impulses, if |μ| > μo then sliding occurs

$$\mu(xc,yc,\beta,\alpha) := \frac{D\zeta(xc,yc,\beta,\alpha)\cdot\eta dot(\beta,\alpha) - K\zeta(xc,yc,\beta,\alpha)\cdot\zeta dot(\beta,\alpha)\cdot(1+e)}{K\eta(xc,yc,\beta,\alpha)\cdot\zeta dot(\beta,\alpha)\cdot(1+e) - D\eta(xc,yc,\beta,\alpha)\cdot\eta dot(\beta,\alpha)}$$

$$\mu o := sign(\mu(xc,yc,\beta,\alpha))\cdot|\mu o|$$

Final velocity in η direction if sliding

$$\eta T(xc,yc,\beta,\alpha) := \eta dot(\beta,\alpha) - \frac{K\zeta(xc,yc,\beta,\alpha)+\mu o\cdot K\eta(xc,yc,\beta,\alpha)}{D\zeta(xc,yc,\beta,\alpha)+\mu o\cdot D\eta(xc,yc,\beta,\alpha)}\cdot\zeta dot(\beta,\alpha)\cdot(1+e)$$

Energy loss from Sticking

$$E\zeta(xc,yc,\beta,\alpha) := \frac{1}{2}\cdot\frac{1}{D\zeta(xc,yc,\beta,\alpha)+\mu(xc,yc,\beta,\alpha)\cdot D\eta(xc,yc,\beta,\alpha)}\cdot\left(1-e^2\right)\cdot\zeta dot(\beta,\alpha)^2$$

$$E\eta(xc,yc,\beta,\alpha) := \frac{1}{2}\cdot\frac{1}{\frac{1}{\mu(xc,yc,\beta,\alpha)}\cdot K\zeta(xc,yc,\beta,\alpha)+K\eta(xc,yc,\beta,\alpha)}\cdot\eta dot(\beta,\alpha)^2$$

Energy Loss from sticking

$$Estick := E\zeta(xc,yc,\beta,\alpha)+E\eta(xc,yc,\beta,\alpha)$$

$$Estick = 224.271\,MJ$$

Energy loss from Sliding

$$E\zeta s(xc,yc,\beta,\alpha) := \frac{1}{2}\cdot\frac{1}{D\zeta(xc,yc,\beta,\alpha)+\mu o\cdot D\eta(xc,yc,\beta,\alpha)}\cdot\zeta dot(\beta,\alpha)^2\cdot\left(1+e^2\right)$$

$$E\eta s(xc,yc,\beta,\alpha) := \frac{1}{2}\cdot\frac{1}{\frac{1}{\mu o}\cdot K\zeta(xc,yc,\beta,\alpha)+K\eta(xc,yc,\beta,\alpha)}\cdot\left(\eta dot(\beta,\alpha)^2-\eta T(xc,yc,\beta,\alpha)^2\right)$$

Energy Loss from sliding

$$Eslide := E\zeta s(xc,yc,\beta,\alpha)+E\eta s(xc,yc,\beta,\alpha)$$

$$Eslide = -42.862\,MJ$$

Energy Loss

If lμl<μo energy loss is from sticking, otherwise it is from sliding

$$E(xc,yc,\beta,\alpha) := \begin{cases} E\zeta(xc,yc,\beta,\alpha)+E\eta(xc,yc,\beta,\alpha) & \text{if } |\mu(xc,yc,\beta,\alpha)| < |\mu o| \\ E\zeta s(xc,yc,\beta,\alpha)+E\eta s(xc,yc,\beta,\alpha) & \text{otherwise} \end{cases}$$

Energy loss from ship collision

Use this result ==> $E(xc,yc,\beta,\alpha) = 224.271\,MJ$

Initial Total Kinetic Energy

$$Ei := \left[\frac{1}{2}\cdot(1+max)\cdot Ma\cdot\left(Vax^2+Vay^2\right)\right]+\frac{1}{2}\cdot(1+mb1)\cdot Mb\cdot\left(Vb1^2+Vb2^2\right)$$

$$Ei = 305.146\,MJ$$

Released Energy Ratio (compared to initial total energy)

$$Er := \frac{E(xc,yc,\beta,\alpha)}{Ei}$$

$$Er = 0.735$$

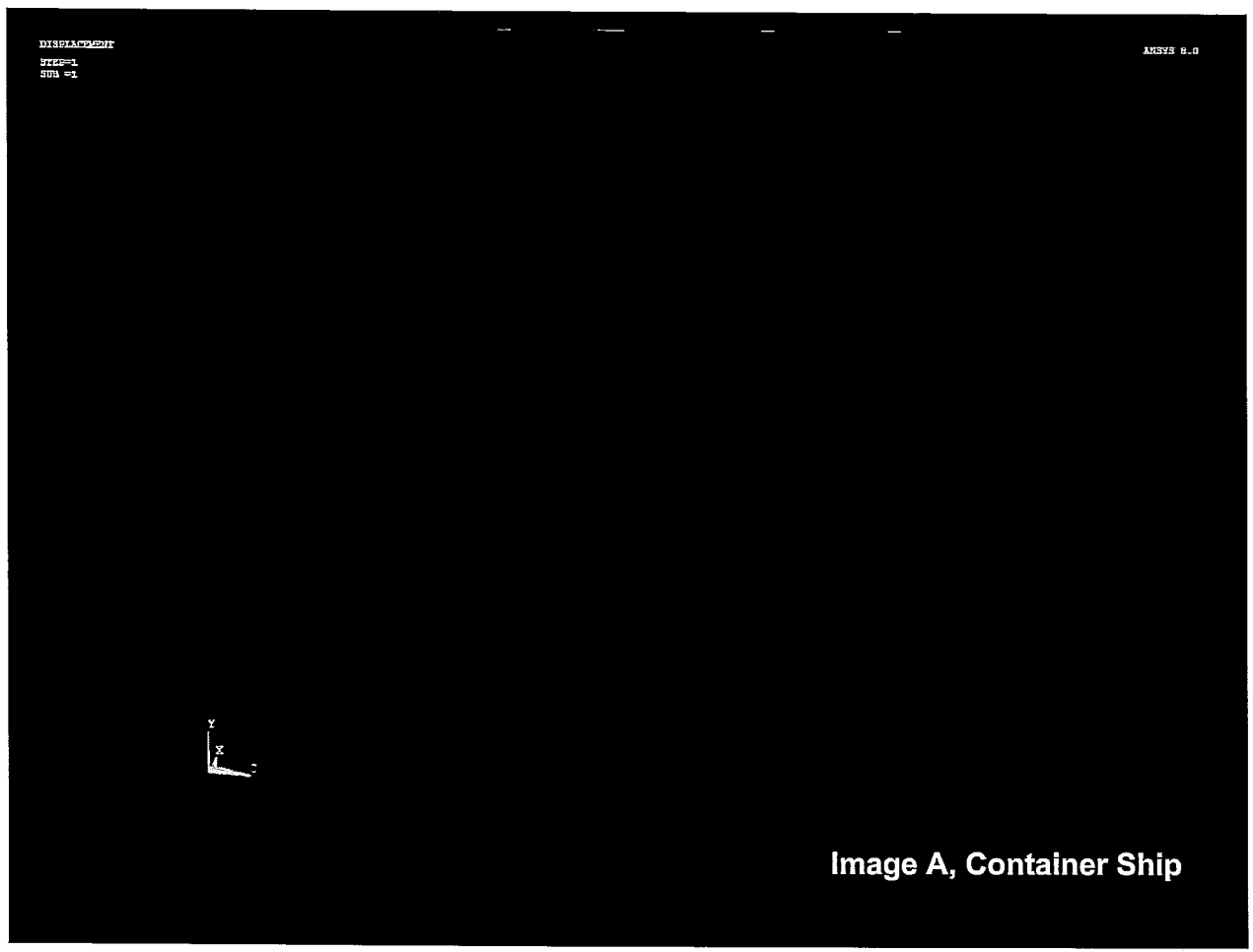

Image A, Container Ship

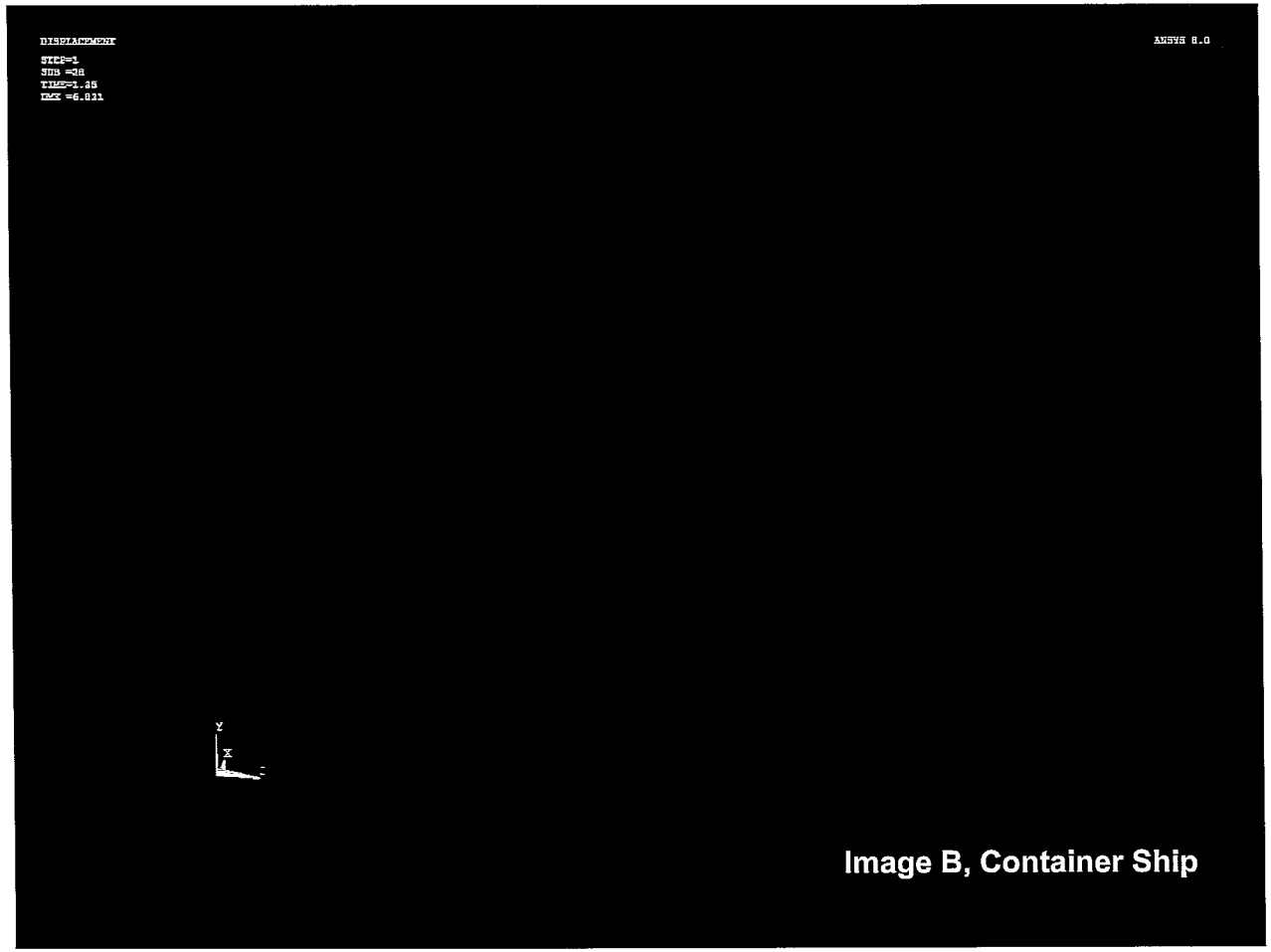

Image B, Container Ship

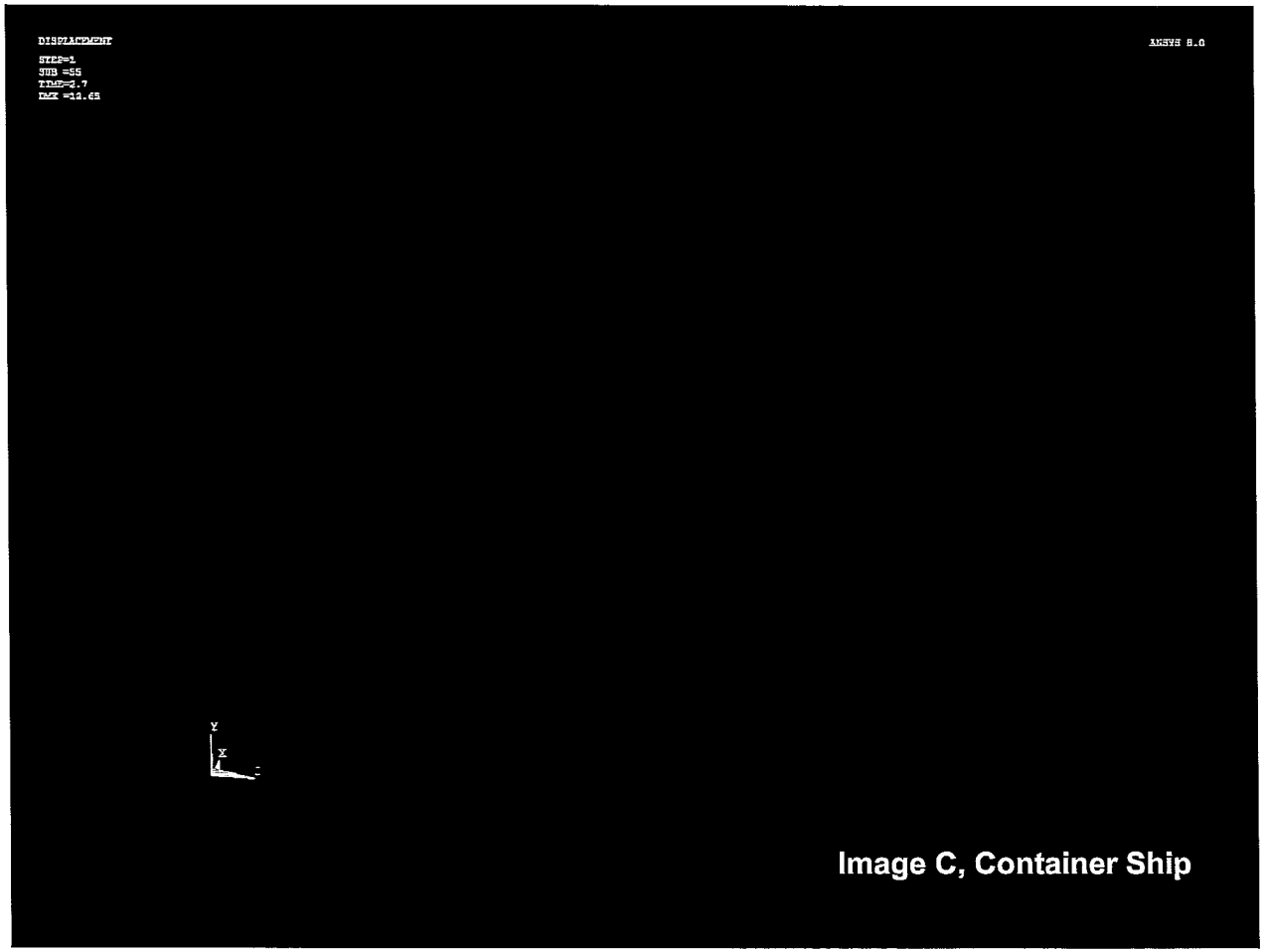

Image C, Container Ship

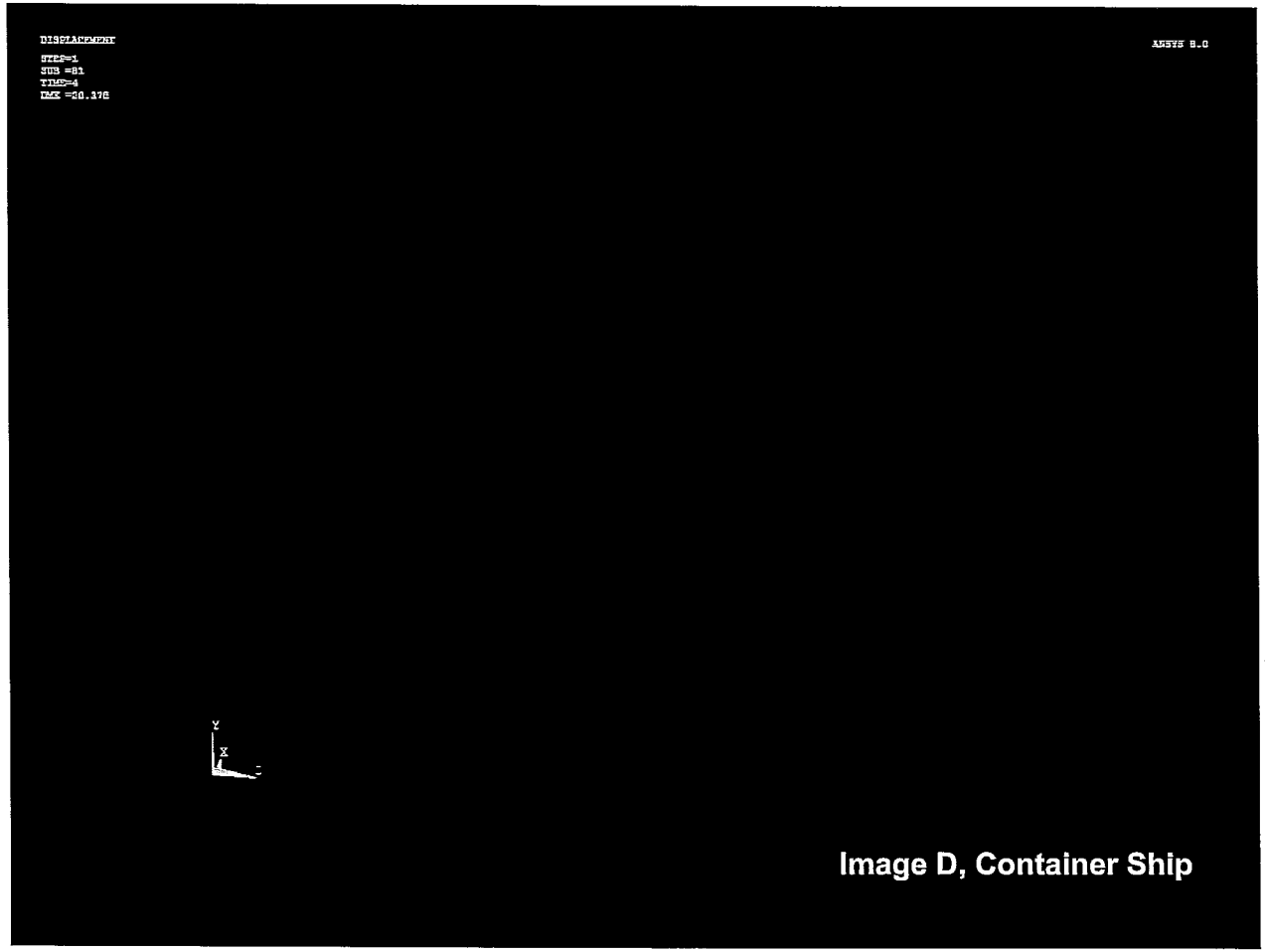

Image D, Container Ship

Image A, FSRU (Container Ship Case)

Image B. FSRU (Container Ship Case)

Image C, FSRU (Container Ship Case)

Image D, FSRU (Container Ship Case)

APPENDIX E
COLLISION ANIMATIONS

THIS PAGE INTENTIONALLY LEFT BLANK